Journal of Nondestructive Evaluation (2025) 44:68
https://doi.org/10.1007/s10921-025-01195-9

A Review of Ex-situ, In situ and Artificial Intelligence-based Thermographic Measurements in Additively Manufactured Parts

Manuela Galati[1] · Simone De Giorgi[1] · Giovanni Rizza[1] · Emanuele Tognoli[2] · Giulia Colombini[2] · Lucia Denti[2] · Elena Bassoli[2] · Luca Iuliano[1]

Received: 6 February 2025 / Accepted: 25 April 2025

Abstract
Additive manufacturing (AM) encompasses a range of advanced production methods that are increasingly applied across various sectors, particularly where customisation, high-strength materials, or complex parts are required. However, a key challenge remains the need for rapid methods and non-destructive testing (NDT) technologies to ensure part quality, particularly for detecting internal defects. Among these methods, infrared thermography (IRT) is gaining popularity due to its ease of use and low overall system cost (hardware, data acquisition, and processing) when compared to more complex techniques like tomography. AM can greatly benefit from IRT, both ex-situ for quality control and in-situ for process monitoring. This paper reviews the current literature on the application of IRT in the AM field. It examines IRT as a standard method for detecting typical defects in AM parts ex-situ, after the manufacturing process. The effectiveness of IRT techniques is evaluated in terms of their ability to detect defects based on size and depth. The paper also explores the use of IRT for in-situ process monitoring, where thermograms are captured during production and analysed to identify defects early. The advantages and limitations of IRT are discussed and compared with other NDT techniques. Additionally, the use of numerical simulation and artificial intelligence (AI) in enhancing IRT applications is reviewed. The findings highlight that while IRT is a valuable tool for defect characterisation in AM, significant potential remains for developing more advanced and efficient approaches that integrate data from multiple sources.

Keywords Additive manufacturing · Infrared thermography · Simulation · Artificial intelligence · Calibration

1 Introduction

Additive manufacturing (AM), as defined by ASTM 52900–2021, refers to a process of joining materials to create objects from 3D model data, layer upon layer, as opposed to subtractive manufacturing methodologies. To produce a part with AM techniques, it is necessary to have a 3D object model in a CAD environment, which is subsequently sliced using parallel planes to obtain the 2D sections which, through overlapping, compose the final shape of the object [1]. The distance between two slicing planes is called the layer thickness. During an AM process, the material is deposited, sintered, or melted according to the 2D section, layer after layer, until the part is completed. AM technologies can work for a large range of materials, e.g. polymers, metals, and ceramics. The layer-by-layer approach in AM offers numerous advantages that have revolutionised part production with a transformative potential across a wide range of industries [2]. One significant benefit is the ability to create complex geometries, including intricate internal channels and lattice structures, which are difficult or even impossible to achieve with traditional manufacturing methods. This approach is also highly efficient, as material is added only where necessary, reducing waste and enhancing sustainability [3]. Furthermore, it facilitates the production of customised parts on demand, enabling tailored solutions for specific applications or individual requirements without incurring significant additional costs [4]. The process supports rapid iteration, allowing designers to modify 3D models and quickly translate these changes into physical parts without retooling or the need for new moulds. Additionally,

✉ Manuela Galati
manuela.galati@polito.it

[1] Dipartimento Di Ingegneria Gestionale E Della Produzione, Politecnico Di Torino, Turin, Italy

[2] Dipartimento di Ingegneria "Enzo Ferrari", Università Degli Studi Di Modena E Reggio Emilia, Modena, Italy

Published online: 09 June 2025

the precise control over the build process can improve the material microstructure and mechanical properties, resulting in enhanced performance in certain applications [5]. The layer-by-layer method also allows for the integration of different materials or functional elements within a single component, opening new opportunities for innovative and multifunctional designs. Despite the increasing adoption in several sectors, particularly aerospace, automotive and medical, the part qualification remains a critical challenge where safety and reliability are paramount [6, 7]. A key focus of qualification efforts is the evaluation of defects and overall quality, which requires a comprehensive approach to ensure that AM parts meet stringent performance standards. This control may be facilitated by the layer-by-layer approach because it enables the integration of advanced quality assurance techniques directly into the process with the aim to track the defect creation during the part construction. Overall, therefore, in the AM chain is possible to apply techniques for in-situ monitoring during fabrication and non-destructive testing after production which are essential for identifying voids, cracks, and other irregularities. Among these, infrared thermography (IRT) has emerged as a powerful tool for detecting defects such as delaminations, voids, and cracks. IRT works by monitoring the thermal response of a part under controlled conditions, providing rapid, non-contact evaluations of surface and near-surface irregularities. In-situ IRT can be used in a particular way in AM using the temperature variation during the process, while a growing interest in ex-situ IRT has also been demonstrated by the introduction of this technique into the recent ISO/ASTMTR52905 for the NDT quality control of AM parts [8]. The main advantages of thermography over other NDT testing are low cost and the opportunity of identifying defective parts early in the process, thereby reducing waste and unnecessary post-processing operations. Research on how to appropriately adapt and calibrate thermography for AM purposes has been growing because of the variety of AM processes and the resulting complexity of the manufactured objects.

This paper provides a comprehensive review of the current state of thermography in the AM field to evaluate its potential in AM applications as a robust, sustainable, and cost-effective non-destructive testing method.

The paper is organised as follows. Section 2 presents the typical defects in AM part and how they are formed. Section 3 summarised the fundamentals of thermography, including differentiation in the performance of IRT, the sources that can be used to perform an active thermography and how IR camera data can be interpreted. The main fields of the applications of the IRT technique are also reported, albeit briefly. Section 4 offers a complete overview of the ongoing research on the application of thermography for the inspection of additively manufactured parts (i.e. ex-situ thermography) and process monitoring (i.e. in-situ thermography). The data are summarised using tables and figures that help in proving an overview of the literature achievements and results. Moreover, the modelling and simulation of the IRT process are discussed. Artificial intelligence (AI) methods used to address the elaboration and analysis of complex thermographs are considered. Studies in which thermography is compared or used jointly with other NDT techniques are also mentioned to highlight differences, potentialities and limitations. Section 5 gives the overall conclusions and presents the future challenges of using IRT in the AM field.

2 Defects in AM

Defects in an AM part may be caused by several phenomena. The detection of such defects generally depends on their morphology, size and geometry rather than their origin [8]. Given the diversity of AM techniques regarding physical phenomena and processing conditions, it is essential to classify the most relevant defects and how they can be detected properly.

Porosity refers to a set of internal pores within a material. These pores can contain, e.g., unmelted powder, gases, or binders, depending on the used process [9, 10]. The morphology of such pores can vary from small and spherical to irregular and elongated.

The voids are usually categorised as either gas-induced or process-induced. Gas-induced porosity is caused by phenomena that occur during the AM process or gas entrapped during the preparation of the raw materials. For example, in AM processes on metals, inert gas may remain entrapped when the particles solidify during powder atomization. These voids are spherical, and typically in the 10 µm to 80 µm range [11, 12]. Gas inclusions, such as hydrogen pores, may form due to differences in solubility between solid and liquid metal. These pores, which often occur in aluminium, titanium and iron alloys, are usually spherical and in the 5 µm to 20 µm range [11, 13, 14]. In AM for polymers or composites, air bubbles can be trapped in liquid resins, where they can reach a millimetric size, or inside the polymer filaments [15–17].

Process-induced porosity arises from an excess of energy, which leads to keyhole porosity, or insufficient energy, which results in a lack of fusion (LOF).

Keyhole porosity involves the formation of a deep vapour cavity within the melt pool, characterised by a distinctive"J"shape, with an average width of 100 µm and a depth of 300 µm, which result in a greater width-to-depth ratio than 1:2. When this cavity collapses, it creates spherical pores that are approximately 100 µm in diameter [11, 14, 18].

LOFs are due to an incomplete bonding, which causes an irregular void formation. These defects can occur between adjacent melted (or deposited) lines, due to a missing overlap of material, or between layers when the energy or the temperature of the deposited material is insufficient to guarantee bonding between two subsequent layers. Moreover, spatter particles that absorb energy intended for the powder bed result in internal voids. LOF defects are generally large and irregular, and they pose great risks under mechanical stress. The dimensions in metallic AM parts may be over some hundreds of micrometres (lengths from 400 µm to 600 µm and heights from 140 to 240 µm) [9, 11, 14, 19, 20]. Similar issues are observed in ME processes, where voids that formed due to a poor nozzle geometry or inadequate extrusion conditions may cause pores of some millimetres in size [21].

Balling defects form when the molten material breaks into spheroids, which are called"balls". In the case of metallic AM parts, this defect is usually generated by incorrect process parameters or poor powder wetting. The average size of the spherical domains is around 150 µm to 250 µm, and such defects lead to rough surface finishing but also to porosity with similar dimensions [22].

Inclusions consist of foreign debris in the build environment, and they interfere with the consolidation process and contribute to porosity [13, 23].

Delamination is caused by an insufficient interlayer adhesion, and it leads to the separation of layers, particularly in metal AM and stereolithography [24–26].

Cracks that form through solidification or in the solid state, due to temperature gradients, accumulated stresses or reduced ductility, have a significant impact on the integrity of the parts. When these defects are present in metal AM, they are usually in the 150–200 µm long and 60–70 µm wide range [13, 27]. Cracks in binder jetting parts are mainly caused by high shear stresses during powder distribution and in the stereolithography process, where the mechanisms that lead to delamination also contribute to crack formation [26].

3 Fundamentals of Thermography

IRT is the study of infrared radiation (IR) emissions [28–31] in a wavelength that ranges from 0.75 µm to 1000 µm, that is, between visible light and microwaves. IR radiations are emitted by every object above 0 K [28, 32]. The correlation between radiance and temperature is governed by Planck's law, in which emissivity is treated as a wavelength-dependent optical property of the material. Thermographic measurements typically rely on the spectral radiance described by Planck's law, especially when materials are not in thermal equilibrium or when narrow-band detectors are used. Under thermal equilibrium, a fixed temperature implies consistent IR radiation emission, and this correlation can be expressed through the material's emissivity using Stefan–Boltzmann's law [33], which is the integrated form of Planck's law over all wavelengths. In contrast, non-equilibrium conditions lead to temperature gradients within the object, resulting in varying IR emissions. Moreover, IR emissions depend on various factors, such as geometry, material density variations, thermal conductivity, and surface emissivity. Variations in IR radiation within the same component may therefore indicate sub-surface non-homogeneities, for instance, at interfaces between different materials. Despite an IRT measurement involves several complex key components working in tandem, the main points are (Fig. 1) [30]:

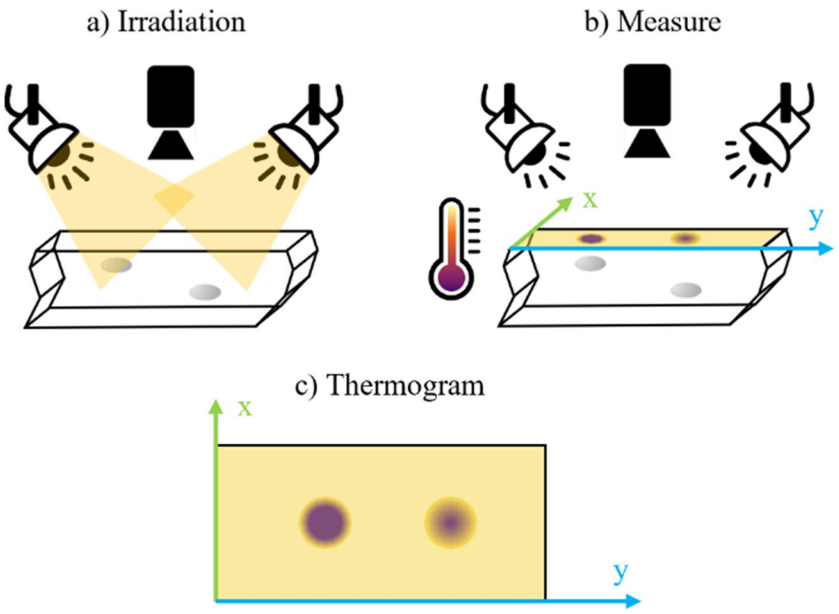

Fig. 1 Basic principles on how a thermogram is produced

- the irradiation source
- the detection system, usually an infrared camera or sensor, capable of capturing and registering the emitted infrared radiation. This system creates a thermal image, also known as a thermogram, which represents the temperature distribution across the object's surface
- an analytical system that processes and interprets the detected data. This system is responsible for analysing the thermal images, identifying anomalies or variations in temperature, and determining the presence of defects or material inconsistencies. The effectiveness of the IRT measurement relies on the precise coordination of these components, with the quality of the irradiation, the sensitivity of the detection system, and the sophistication of the data analysis all playing critical roles in ensuring accurate results.

When the non-thermal equilibrium condition is natural, the phenomenon can be studied as it is, and this approach is called passive thermography. Therefore, in passive thermography, the temperature distribution of a component is recorded without any external thermal stimulation, as the object serves as the heat source [28, 31]. The features of interest in passive thermography naturally exhibit temperatures that are higher or lower than the surrounding background [31].

The passive thermography method is effective when the part that has to be analysed undergoes inherently significant thermal variations. Passive thermography is generally used in quality control and process monitoring [33] and can be applied to various scenarios. It is exploited in the construction field to inspect civil structures [28, 33] and cultural monuments, using a solar load cycle [33] to detect moisture [33], insulation [33, 34] or seepage problems in buildings [34]. Various relevant examples can also be found in the literature referring to the monitoring of the health of rotor blades [35], the monitoring of generalised corrosion [36] and in pipe walls in thermal power plants [34], to the inspection of aircraft structures to detect water in panels [33] and to the monitoring of the condition of machinery [28]. In addition, monitoring with passive thermography is essential to achieve optimal results in industrial processes that involve high temperatures, e.g. rolling [33], sintering [33] or welding [28]. Mechanical testing can benefit from the use of this thermographic method, for example, to monitor the damage and thermomechanical behaviour of composite materials [37] and to monitor deformation under tensile and fatigue loading [28]. The monitoring of electrical and electronic components [28, 33] and the measurement of power dissipation in electronic chips [34] are two examples of the applicability of passive thermography for electrical purposes. Additionally, the passive method is also used in the field of medical sciences to identify emphasise skin diseases [38]. In all these applications, the advantages of the passive approach concern the ease and simplicity of conducting experiments and of analysing the data [28, 34]. On the other hand, the main disadvantage of passive thermography is that it cannot provide a clear thermal contrast between the anomalies within a part and its surroundings that can be used to detect deep subsurface defects; moreover, its capacity for quantitative analyses is somewhat limited [34].

To overcome this issue, there is the need of creating a non-thermal equilibrium condition using an external heating source. In this case, the analysis is called active thermography [29]. Therefore, active thermography necessitates an external excitation source to thermally stimulate the part under examination [31]. Heating sources (Table 1) can be optical, that is, when the object is heated using lasers, flash lamps or halogen lamps; microwave; from an electric current using the Joule effect; inductive from an eddy current; convective by investing the object with liquids or gases; or mechanical, which involves generating heat using vibrations [30, 33]. Each source has specific benefits and weaknesses as summarised in Table 1, and it should be chosen according to the material of the component and the defect to be detected.

Table 1 Summary of the key strengths and weaknesses of the reviewed excitation methods

Active thermography techniques	Main strengths	Main weaknesses
Optical flash stimulated technique	- Possibility of inspecting large areas	- Difficulty in detecting microdefects - Limited robustness
Optical laser stimulated technique	- High level of accuracy	- Inspection point by point, slow speed
Convective heat stimulated technique	- Low cost - Suitable for cavities	- Slow heating - Low level of repeatability
Eddy current stimulated technique	- High levels of reliability and reproducibility	- Limited to electrically conductive materials
Electric current stimulated technique	- Time and cost effective - High SNR - Possibility of detecting sub-surface defects	- Limited range of electrically conductive materials - Challenging contact setup
Microwave stimulated technique	- Fast volumetric heating	- Safety limitations
Mechanically stimulated technique	- Simple and straightforward analysis - Possibility of detecting medium-depth defects	- Challenging contact setup - Risk of part damage

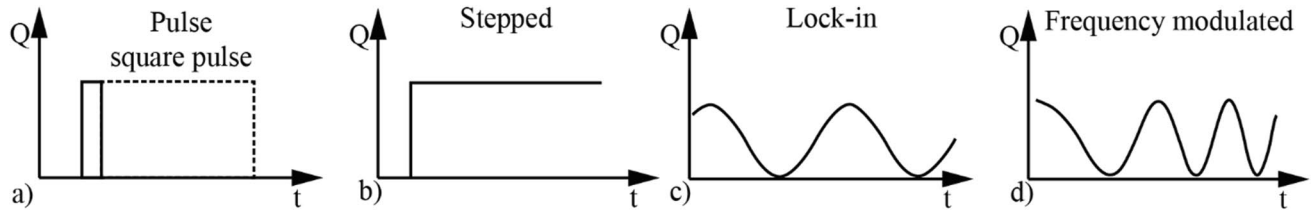

Fig. 2 Type of excitation functions: (**a**) Pulse and Square Pulsed thermography, (**b**) Stepped thermography, (**c**) Lock-in thermography, and (**d**) Frequency modulated thermography

All these sources can be supplied with different temporal evolutions (See Fig. 2), such as pulsed, when the energy is provided instantaneously, stepped, when the supply of energy is continuous, or lock-in, when the thermal excitation is periodic [31]. Therefore, differently from passive thermography that is generally stationary, active thermography is typically non-stationary or dynamic [39]. Therefore, active thermography is classified differently, according to the heating source, the excitation function, the relative position and movement between the part and the energy source, the scanning method and the type of heating, as proposed by Yang & He [31] (Fig. 3).

The source can distribute the heat within the component with several methods (Fig. 3) [31]. The heating mechanisms will affect defect temperature, which may appear as cooler or hotter regions in infrared imaging depending on the defect type. Surface heating thermography (SHT), shown in Fig. 4a, heats the component's surface and detects defects through heat conduction and reflection [31]. SHT methods include optical flash and laser-stimulated thermography and eddy current or electrical current-stimulated thermography for conductive parts [31, 40]. Volume heating thermography (VHT), depicted in Fig. 4b, heats the entire component, with defect detection based on conductivity changes [31]. VHT methods, such as flash-stimulated thermography in transmission mode and eddy or electrical-current thermography for low-conductivity materials, offer deeper penetration than SHT [40]. Microwave-stimulated thermography can also be VHT for dielectric materials [41]. Generative heating thermography (GHT), shown in Fig. 4c, selectively heats defects while leaving the surrounding material unaffected [31]. Mechanically stimulated thermography, including ultrasound and eddy current methods, is considered GHT when applied to CFRP and water detection in concrete [41, 42].

Also, the position (Fig. 5) and movement of the excitation source and the camera (Fig. 6) respect the object are also additional characteristics of the design of the whole IRT measurements [31, 43]. In reflection mode (one-sided technique), both the energy source and camera are on the same side, making it practical for parts where access to both

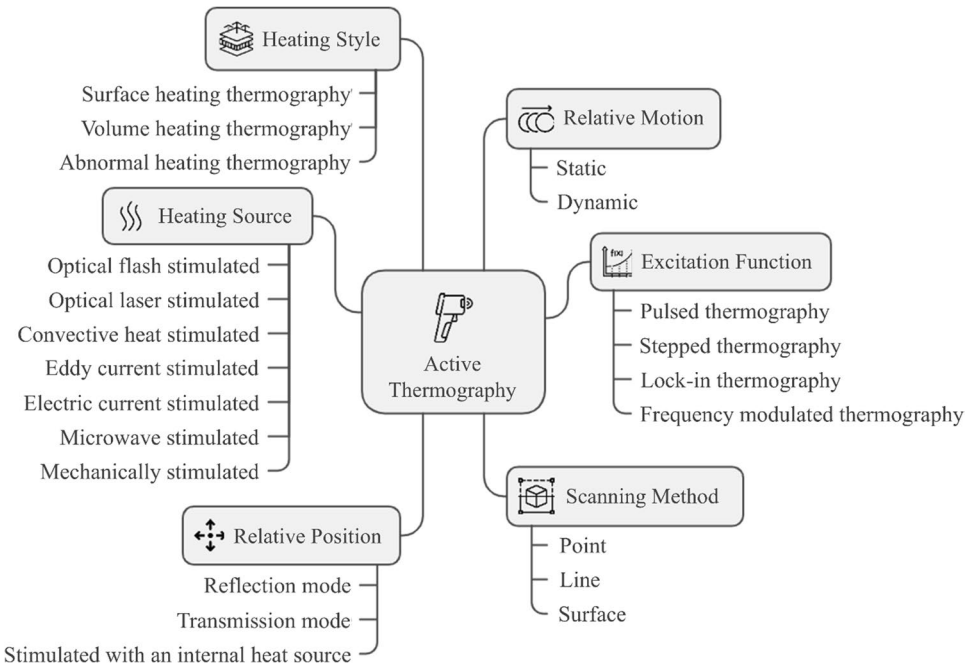

Fig. 3 Classifications of active thermography

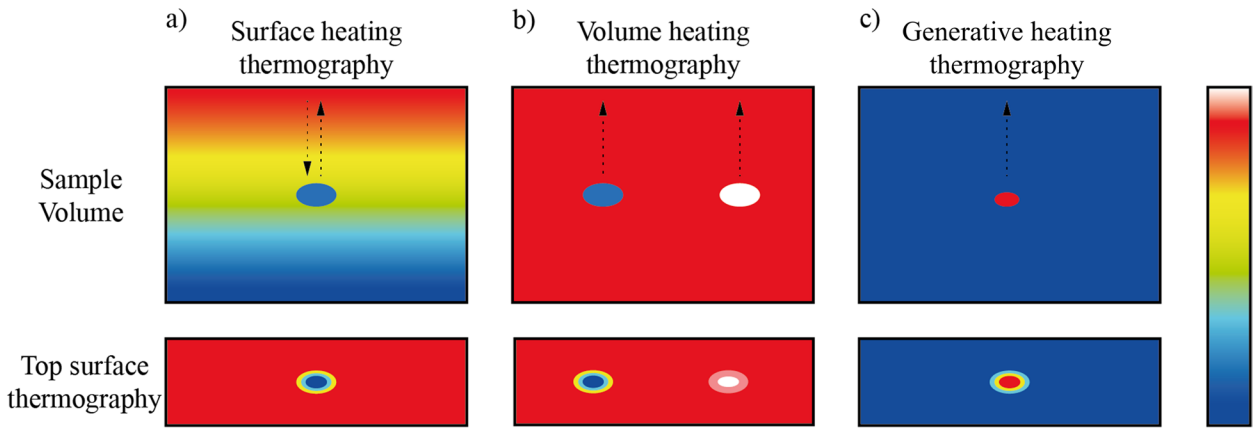

Fig. 4 Different heating modes: (**a**) Surface heating, (**b**) Volume heating, and (**c**) Generative heating thermography

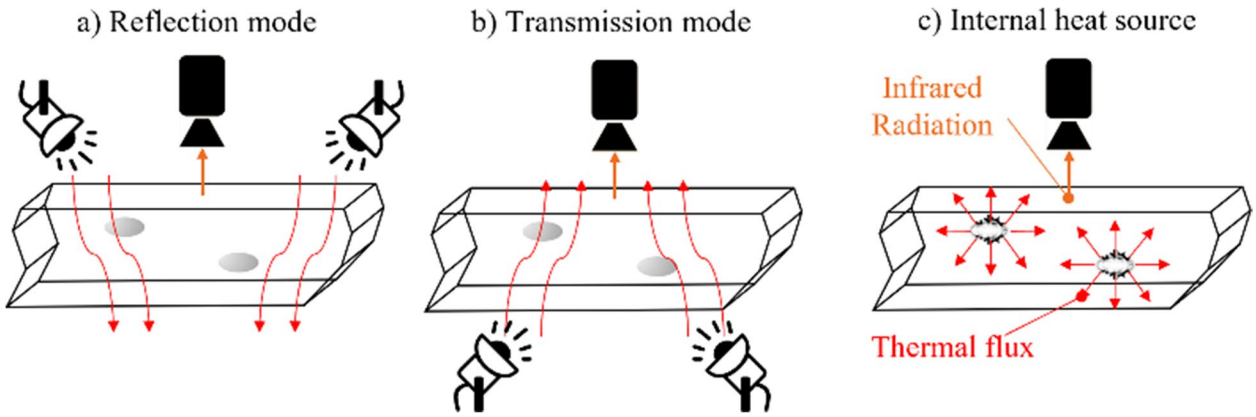

Fig. 5 Relative position between a part and a source

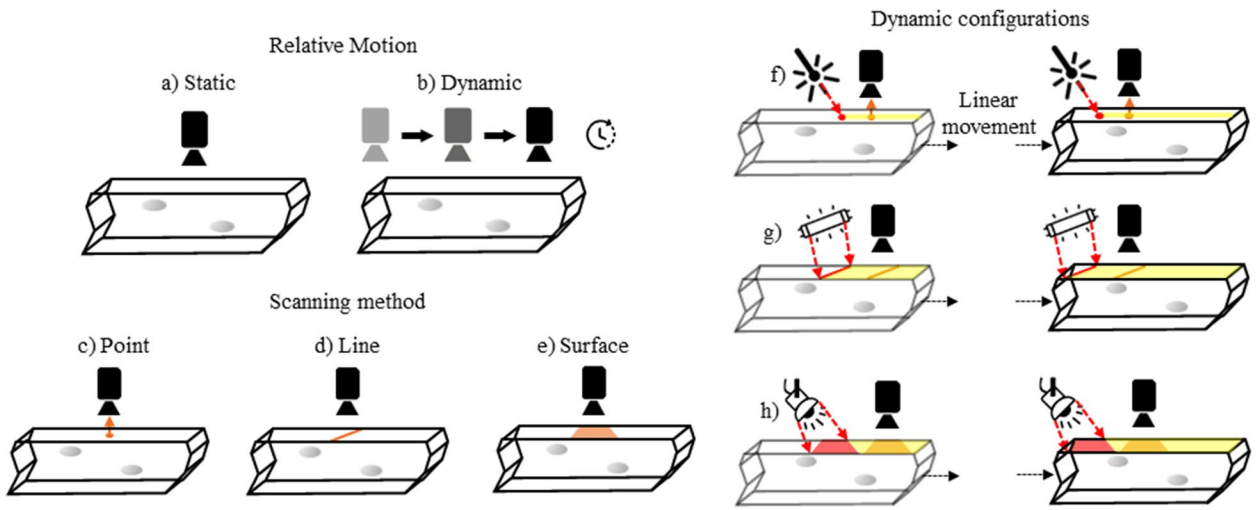

Fig. 6 Different thermography setups, depending on the relative motion between the camera and sample

sides is restricted [31]. This mode is particularly effective for detecting surface-near defects and allows depth quantification in optically stimulated thermography [31]. In transmission mode (two-sided technique), the source and camera are on opposite sides of the part, requiring heating through the sample, which limits its use for thick or insulating materials [43]. However, it provides more accurate results for thin components and detects deeper defects across the sample thickness [30, 43]. The excitation source does not block the camera's view [31]. Thermography can be static or dynamic, based on movement during the inspection [30, 31]. Static configurations keep all elements stationary, which is useful for precise data tracking but impractical for large or complex parts. Dynamic configurations speed up inspections, with at least one element moving [30, 31] that can scan the surface. The scanning methods include point scanning (using a localised heating device and IR camera), line scanning (heating with a line projection for faster inspections), and surface scanning (heating and monitoring a large area, often used in static setups) [30, 31, 43]. Point and line scanning are used in dynamic configurations [30]. Various configurations combine movements and scanning methods, such as point scanning with a rotating part or surface scanning with moving elements [43].

Active thermography is generally preferred over the passive approach as it offers certain quantification capabilities and produces a higher thermal contrast, which improves the possibility of analysing deeper layers within the inspected part. This makes it a valuable technique for inspections that require a thorough depth analysis [34]. Because of that, active thermography techniques are predominantly utilised to detect and quantify defects in various materials, including metallic [44–47], polymeric [48] and concrete [49] ones. The literature has recorded numerous industrial applications of active thermography, such as the detection of blisters in the corrosion-protection coating of oil tanks [50], the inspection of rail samples [51], the evaluation of the quality of weld seams [52], the detection of delamination [53] and inlays in layered structures for the automotive and aerospace industry [54]. Other applications include assessing metal corrosion [55], inspecting composite laminates [56, 57], identifying defects in honeycomb sandwich structures [58], and detecting microcracks in aluminium components for the aerospace sector [59]. In recent years, active thermography has been increasingly used to detect naturally or artificially induced defects in parts manufactured via AM, particularly powder bed fusion (PBF) [60–62]. In addition, direct monitoring (in-situ) of the PBF process has garnered attention, due to its potential to detect and prevent defects during production [63–65].

An electronic IR camera is generally required to perform a thermographic study. The main components that constitute such a device are IR detectors, lenses, an optional cooling system, an ambient temperature sensor, an electronic unit, a display, and software. The IR detectors can be arranged in a matrix, which is called Focal Plane Array (FPA). The most common type of IR detector is the microbolometer, which exploits the bolometric effect. In this case, the electrical resistance is modified by the temperature detected in the microbolometer sensing element. The variation of the electrical resistance is measured by means of electronics and converted into a numerical value that corresponds to the estimated temperature of the object. This conversion is carried out with calibrated parameters, such as emissivity, object distance, ambient humidity, and temperature. A collection of the numerical values results in a false-colour image, called "thermogram", in which each pixel corresponds to a microbolometer measurement. A large number of IR detectors results in a better resolution. This parameter specifies the number of microbolometers that are present and how the matrix is arranged. For example, an IR camera, characterised by a resolution of 640×480 pixels, contains 640 columns and 480 rows of microbolometers for a total of 307.200 IR detectors. Another parameter that is considered to describe an IR camera is the ratio between the dimension of the sensing element and the distance from the lenses. This parameter is called "instantaneous field of view (IFOV)", and it describes the angular distance between two independent measurements, but also the physical angular aperture of a pixel. The combination of the IFOVs of all the detectors is called "field of view (FOV)", and this represents the total angular opening of the IR camera.

An IR camera is also characterised by other significant parameters, such as the wavelength range at which the sensing element can detect IR radiation. This quantity is called spectral range, and since the wavelength and temperature are connected through Plank's law under black-body conditions, a spectral range directly defines the temperature range that can be detected. In real measurements, objects are considered grey bodies. Therefore, it is important to consider the spectral range and temperature range in which IR cameras can operate optimally, as well as the minimum temperature difference that is detectable (which is called thermal sensitivity or noise equivalent temperature difference—NETD).

A thermogram is a single instantaneous measurement. In order to study a thermal evolution, it is necessary to acquire a certain number of thermograms within a unit of time. The number of thermograms that can be acquired in a second is known as the frame rate.

Each generated thermogram is composed of raw information that needs to be post-processed to increase the so-called signal-to-noise ratio (SNR). SNR is a dimensionless parameter that indicates the difference between a measurement region of interest (ROI) and a reference area. A large SNR indicates the possibility of differentiating the most efficient sound area from ROI and, consequently, extracting

more information. The analysis of thermograms is a time-consuming step and requires a sequence of operations, including acquiring, post-processing and image evaluation. In this regards, the use of artificial intelligence (AI)-based methods is increasing, with the intent of speeding up data elaboration and non-homogeneity recognition [60, 66, 67]. However, few studies have been conducted in this direction, although the interest in large-scale implementation is becoming more and more intriguing. Apart from AI, IRT simulations are also considered a primary tool to reduce the effort when analysing thermograms. Simulating the results of IRT on an object in advance is a precious way of anticipating thermal diffusion and of simplifying data acquisition and post-processing. IRT simulation can also be applied to CAD models to predict thermal behaviour or to investigate the potentiality of IRT, using an object with intentional flaws that has been specifically designed for this purpose.

Regardless of how the information is collected, IR measurements are largely applied for different aims in various fields, such as in the medical, electrical and electronic fields and in construction [28, 29, 43, 68–70]. IRT is also implemented in industrial applications to monitor processes or test and detect defects, anomalies and thermal dispersion. Any manufacturing process which involves thermal reactions can be monitored using an IR camera. The presence of a discrepancy in the thermal distribution can be a warning signal of an inadequate procedure, e.g. cold points of strong thermal gradients that may generate cracks [71]. The application of IRT for monitoring purposes during a manufacturing process is called in-situ thermography [72]. IRT thermography as a non-destructive testing (NDT) method that is applied by inducing a thermal non-equilibrium in an active approach. This technique allows any inhomogeneity e.g. pores, cracks and/or inclusions to be detected, and assists programmed control and quality control after production. In this case, IRT thermography is called ex-situ thermography [73, 74].

3.1 Data Elaboration and Interpretation

Thermograms obtained from IRT often require post-processing, due to certain inherent challenges, such as low surface emissivity and roughness, which lead to a low SNR. An effective detection of defects and the interpretation of the results necessitate the application of specialised algorithms to enhance the SNR. Several algorithms that can be used to refine defect identification and optimise the overall testing procedure exist [33]. Formally, the data from an IRT test can be represented as a three-dimensional matrix of temperature values T (i, j, τ), where the spatial coordinates (i, j) correspond to the surface, and τ indicates discrete time intervals [39]. The data processing techniques can either be one-dimensional or two-dimensional, and can focus either on the temporal temperature evolution at each pixel T (τ), or on specific images T(x,y) [39]. Typical approaches involve filtering or segmenting individual IR images to reduce noise and analyse the geometric features within the areas of interest [39]. The different approaches can be summarised as follows:

- Differential Temperature Signal: Detects temperature differences but is limited by surface emissivity and absorptivity [39, 75]
- Dimensionless Temperature Contrast: Reduces dependence on heating power but amplifies noise and neglects lateral heat diffusion [39, 75]
- Differentiated Contrast Analysis: Requires no reference point but is best suited for flat defects [39, 76]
- Averaging Technique: Reduces noise but ignores material emissivity and absorptivity [39, 75]
- Gapped Smoothing Algorithms (GSA): Detect subsurface defects without a reference, improving contrast and detecting deeper flaws [59, 77]
- Normalisation Techniques: Suppress deterministic noise but amplify random noise [39, 57, 75, 78]
- Temperature-Resolved Radiometry: Extends heating to enhance deeper defect visibility, though surface reflections may impair accuracy [39, 75, 79]
- Early Detection: Focuses on initial signals but has issues with small defect detection [39, 80]
- Fourier and Wavelet Transforms: Suppress non-uniform heating impacts and improve resolution but depend on acquisition settings [33, 39, 60, 75, 78, 81–84].
- Principal Component Analysis (PCA): Identifies spatiotemporal features but is computationally intensive [39, 59, 85]
- Statistical Moments: Highlights defects via temperature distribution changes [33, 86]
- Thermographic Signal Reconstruction (TSR): Reduces noise and improves visibility, particularly for small defects [39, 59]
- Dynamic Thermal Tomography: Provides depth-specific thermal analysis, estimating defect depths with reasonable accuracy [33, 39, 87–89]. Therefore, this method is essentially insensitive to such surface issues as discolouration, texture and shape, as well as to lateral heat flow and heat loss mechanisms, which is why the accuracy can be kept very close to the thermal limits [39]. Like many other methods, it relies on treating samples as semi-infinite bodies and requires a reference point [39]
- Convolutional Neural Networks (CNN) and Data Fusion Use machine learning and combined datasets to enhance defect detection, though challenges remain in standardisation [39, 90–93]

3.2 Applications in the Industrial Field

Thermography is a versatile technology that is applied over a wide range of sectors. IRT is used in agriculture and food [94–96], medicine [38, 97, 98], construction [99–101], aerospace [59, 102, 103], and nuclear industries [104–106].

Industrial applications of IRT techniques have been categorised into two main groups in the literature: electrical and mechanical [68].

In electrical engineering, IRT covers numerous applications in such sectors as industry, the service sector, transport and power generation [68]. In this context, IRT is primarily used for condition monitoring [68]. A classic application is the preservation of electrical installations [107], which includes monitoring the state of electrical switchgear and insulation systems [107, 108]. IRT is also used to detect faults in power converters in industrial plants [109]. Moreover, IRT is used in solar energy applications to assess the degradation of lithium batteries [110] and as a maintenance tool for electrical panels [111]. In some studies, IRT has been used to evaluate excitation winding during the rotation of synchronous generators [112]. IRT has recently been increasingly used to condition the monitoring of rotating electrical machines, especially electric motors, which are widely used in industry [68].

IRT has become an important tool, in the mechanical application field, for the analysis of faults and to complement other defect detection methods [68]. For example, IRT has been used in machining to measure the temperature during machining operations [113]. IRT has been employed to evaluate milling [114] and drilling [115] operations, but also to measure the temperature of chips during the orthogonal cutting of steel and in other machining configurations [116, 117]. In addition, IRT has been used to measure the rake face temperature of cutting inserts to relate it to tool wear [117]. IRT has been used effectively in the field of plastics, in particular to investigate defects in composite materials such as carbon fibre reinforced plastics [118] and damage under fatigue loading [119]. This technique is used for the industrial sintering of plastics to measure the temperature of the sinter during the cooling phase [120]. Other applications include the detection of deformations in metal foams [121] and the identification of defects in metal welding processes [122]. IRT has been used in experimental studies in the railway industry to characterise artificial and natural cracks in steel sheets and rails [123]. In addition, IRT is frequently used to monitor the condition of components in the aerospace [59] and automotive [124] industries.

4 Thermography in AM

4.1 Ex-situ Thermography in AM

The effectiveness of thermography is not only inherently connected to the physical limitations of the technology, but also to the specific characteristics of the IRT methods and the defects within the sample, particularly their size and their depth from the inspected surface. Therefore, a comprehensive quantity that takes both parameters into account, known as the size-to-depth ratio, can be used as a key performance indicator of thermographic capabilities. The empirical rules in IRT suggest that defects with a greater size-to-depth ratio than 2 are easy to detect, but recent studies have lowered this limit to 1 or, in some successful cases, even to 0.5 [47, 125].

The literature on NDT of components manufactured using conventional methods is rich and diverse, for both metallic and polymeric parts. However, the state of the art, in terms of AM applications, is still quite limited, and covering results only for a limited number of sources of excitation for thermographic measurement. A summary of the state of the art of ex-situ IRT used on AM parts is provided in Table 2. The column "Reference defect" describes the typical defect of the additive manufacturing process which the respective bibliographic work aimed to emulate with one or more artificial defects created into the part. Typically, the dimensions and orientation of the defects introduced are such that the defects crosses several hundred layers with a few exceptions of a few tens. It should be noted that in most cases the surfaces examined are painted black or coated with graphite.

For metallic components, the sensitivity of optical flash-stimulated thermography is limited by issues like noise, low SNR, and image blurring, affecting the detection of smaller or deeper defects. Studies have explored machine learning and post-processing algorithms to enhance defect detection in powder bed fusion with laser beam (PBF-LB) manufactured plates with calibrated porosity defects. Results showed large defects were detectable with high accuracy, while smaller ones required advanced algorithms, reaching limits of 127 µm in diameter and depth. Spherical defects with a diameter-to-depth ratio above 3 were detected reliably, with probabilities improving using thermal signal reconstruction techniques. D'Accardi et al. [129] compared flash and laser-stimulated thermography for detecting defects in AM-produced AISI 316L samples. Laser thermography outperformed flash methods, with higher signal background contrast and better detection, especially on graphene-coated surfaces. Smaller defects required advanced post-processing algorithms, highlighting the limitations of thermographic techniques. Other studies, such as Ref. [62, 148] confirmed

Table 2 Summary of the ex-situ IRT studies on AM parts

IR technique	AM technique	Material	Type of defect	Size [mm]	Depth from the surface [mm]	Algorithm	Layer thickness [µm]	Layers affected by defect [n°]	Surface coating	Reference defect	Detection	Ref.
Optical flash stimulated technique	PBF-LB	SS-316L and Inconel 718	Hemispherical hole	1–8	1–5	STBSS and STSDL	20 (SS-316L) 40 (Inconel 718)	25–400 (SS-316L) 13–200 (Inconel 718)	Washable spray graphite paint	Porosity	Yes, up to 4 mm in size	[60]
Optical flash stimulated technique	PBF-LB	SS-316L	Hemispherical hole	1–8	1–5	SC/K-SVD	20	25–400	Washable spray graphite paint	Porosity	Yes, up to 2 mm in size and 1 mm in depth	[126]
Optical flash stimulated technique	PBF-LB	SS-316	Flat bottom hole	0.076–0.203	0.127–0.508	STSCS	/	/	Krylon flat black paint	Porosity	Yes, up to 101 µm located at a depth of 127 µm	[127]
Optical flash stimulated technique	PBF-LB	316L	Hollow spheres	3, 6 and 8	0.2–5	TSR and PCT	30	100–267	/	Porosity	D/d > 4, without the used algorithm; 3 < D/d < 4 with the algorithm	[128]
Optical flash stimulated technique	PBF-LB	Maraging steel and Hastelloy	Open cylindrical voids	0.1–0.7	-	No	/	/	/	Lack of fusion, voids and porosity	Yes, up to 0.4 mm in size	[8]
Optical laser stimulated technique	PBF-LB	316L	Keyhole porosities and LOF	0.25–1	0–0.1	TSR	50	5–20	Graphite	Keyhole porosity and lack of fusion	Yes	[129]
Optical laser stimulated technique	PBF-LB	316L	Keyhole porosities	0.35–6.19	0.5	PPT	50	20	Graphite	Porosity	6.19 and 2.83 mm without the used algorithm; 1.29 and 1.09 mm with the algorithm; 0.35 mm never detected	[74]
Optical laser stimulated technique	PBF-LB	316L	Keyhole porosities and lack of fusion	0.2–0.8	0.4	PPT	50	20	/	Keyhole porosity and lack of fusion	Partial	[130]
Optical laser stimulated technique	PBF	Titanium	Blind holes	0.7	1.3 and 2.7	No	/	/	Matt black paint	Porosity and lack of fusion	Only at a depth of 1.3 mm	[62]
Optical laser stimulated technique	Direct energy Deposition with LB	Iron-based powder	Surface cracks	0.100–0.15 0.002–0.08	-	No	/	/	/	Cracks	Yes, neural network for width estimation	[131]

undefined(continued)

IR technique	AM technique	Material	Type of defect	Size [mm]	Depth from the surface [mm]	Algorithm	Layer thickness [µm]	Layers affected by defect [n°]	Surface coating	Reference defect	Detection	Ref.
Optical laser stimulated technique	Metal additive	Inconel 600	Superficial, blind and through holes	0.2–0.64	0–1.3	No	/	/	Matt black paint	Porosity and Voids	Yes, all the defects	[132]
Mechanically stimulated technique	Metal additive	-	Superficial defect in the transition zone	-	-	-	/	/	Matt black paint	Cracks and delamination	Yes	[133]
Convective heat stimulated technique	PBF-LB	Maraging steel and Hastelloy	Open cylindrical voids	0.1–0.7	-	No	/	/	/	Lack of fusion, voids and porosity	Yes, up to 0.3 mm in size	[8]
Convective heat stimulated technique	PBF-LB	Inconel 718	Open cylindrical voids	0.02–2	0.02–0.08	No	20	1240	/	Porosity and delamination	Yes, up to 300 µm in size; size-to-depth ratio of 25.	[134]
Optical flash stimulated technique	MEX	PLA, CFRP, GFRP and KFRP	Rectangular voids	12×50×0.5	1.38, 2.75 and 4.12	No	800	1	/	Delamination	Yes	[135]
Optical flash stimulated technique	MEX	ABS and PLA	Square voids	8x8 12x12	0.68–1.15	No	/	/	/	/	Yes	[136]
Optical flash stimulated technique	MEX	Polycarbonate	Open holes	-	-	PCT Fourier transform TSR PPT	/	/	/	Delamination	Yes, three out of four	[137]
Optical flash stimulated technique	MEX	PA-12	Square void	10×10×0.5	2.5	No	/	1–3	/	Voids and delamination	Yes	[138]
Optical flash stimulated technique	MEX	PLA	Circular, square and triangular voids	20 and 0.5 thicknesses	2.5	No	/	1–3	/	Voids and delamination	Yes	[139]
Optical flash stimulated technique	MEX	PLA	Delamination	-	1.25, 2.5 and 3.75	No	/	1–3	/	Voids and delamination	One out of three	[139]
Optical flash stimulated technique	MEX	CFRP	Square and circular holes	7	1.25 and 1.5	Yes	350	1–2	/	Porosity and delamination	Yes	[140]
Optical flash stimulated technique	MEX	ABS	Square voids	5, 8 and 10	0.3–1.8	No	/	/	None (printed in black)	/	Yes, up to a depth of 1.2 mm	[141]

Table 2 (continued)

IR technique	AM technique	Material	Type of defect	Size [mm]	Depth from the surface [mm]	Algorithm	Layer thickness [µm]	Layers affected by defect [n°]	Surface coating	Reference defect	Detection	Ref.
Optical flash stimulated technique	MEX	CFRP, Kevlar, hybrid composite	Circular open voids	-	-	No	100–140	/	Matt black paint	Delamination	Yes, two out of three	[142]
Optical flash stimulated technique	MEX	PLA	Square voids	20 and 30	3–5	Da Silva TSR	250	8–12	/	Voids	30mm in size at any depth; 20 mm in size at a depth of 3 mm	[143]
Optical flash stimulated technique	MEX	CFRP	Square and circular voids	3–10	0.25–2	PCA	140	1–20	/	Porosity and delamination	Yes	[144]
Optical flash stimulated technique	MEX	PLA and PA-12	Square voids	5, 10 and 15	2.55–2.85	TSR	300	1–3	/	Voids	Yes, all of them	[145]
Optical flash stimulated technique	MEX and PBF-LB	ABS and PA 12	Cylindric defects	2–8	0.2–3.9	TRS and FFT	100–600 (ABS) 60–200 (PA 12)	1–6 (ABS) 1–10 (PA 12)	Blackened	Voids	Yes, up to 3 mm in size at a depth of 3.7 mm	[146]
Optical flash stimulated technique	MEX	PLA	FBH, disc and sphere	1, 3 and 5	0.3–3.3	TSR and NLF	/	/	/	Voids	Yes, up to 1 mm at 1.05 mm, to 3 mm at 2.4 mm and to 5 mm at 3mm	[147]

the potential of laser thermography for localising defects but noted challenges in accurately measuring their size and depth. As can be observed from the table, the number of studies for other sources are extremely limited. Only one work has been found regarding the used of mechanically stimulated thermography [133]. In this work, Chulkov et al. [133] tested a hollow, bottle-shaped metal part with a metallurgical discontinuity using ultrasound at 22 kHz. Coated with black paint for better emissivity, the part showed a 1 °C temperature difference in defective areas, confirming the technique's sensitivity to small discontinuities while the surrounding material maintained uniform temperature. Kolb et al. [134] used convectively stimulated thermography to detect defects in an Inconel 718 sample produced by PBF-LB. The technique detected open defects as small as 300 µm but was ineffective for smaller ones. Despite this, it was fast and effective for shallow sub-surface defects. ASTM's report [8] tested a star-shaped artefact with defects ranging from 0.1 mm to 0.7 mm in diameter. Optical flash and convective step heating thermography both detected open surface defects, with convective heating identifying defects as small as 0.2 mm, though both methods struggled with deep-seated defects.

Besides the metallic materials, IRT studies are growing particularly for polymeric parts. Silva et al. [135] used optical flash-stimulated thermography to detect defects in composite Material Extrusion (MEX) fabricated PLA parts, successfully identifying defects in CFRP, GFRP, PLA, and KFRP. The highest thermal contrast was found in CFRP, followed by GFRP, PLA, and KFRP. In contrast, Pierce et al. [136] studied ABS and PLA with defects of 8 mm and 12 mm at depths between 0.68 mm and 1.15 mm, where defects were detected, but thermal contrast was below noise levels, suggesting longer pulses could improve detection. Metz et al. [146] examined PA 12 and ABS with defects ranging from 2 to 8 mm and depths from 0.2 mm to 3.9 mm. ABS showed higher detectability due to better effusivity contrast compared to PA 12. Shagdyrov et al. [142] observed damage in CFRP, Kevlar, and hybrid composites, showing varying thermal inertia with impact energy. Carvalho et al. [138] found reflection mode more effective for early defect detection in PA-12, while Machado et al. [139] noted that reflection mode provided higher resolution but suffered from uneven heat distribution. Notebaert et al. [140] confirmed the recognition of defects in CFRP plates, while Saeed et al. [144] detected defects in CFRP samples, showing the effectiveness of the method with algorithms to improve detection. Rodríguez-Martín et al. [145] found larger defects more visible, but with some thermal measurement inaccuracies. A study on infill percentage by Rodríguez-Martín et al. [137] showed that higher infill reduced defect detection probability, while Santana et al. [143] found smaller, deeper defects less detectable in PLA with lower infill, emphasizing the influence of thermal gradients on detectability.

Comparing these studies, it is clear that thermal contrast, material properties, and infill levels significantly influence the effectiveness of defect detection.

Figure 7 and Fig. 8 provide a graphical overview of the detection possibilities, in terms of minimum size and maximum depth of defects in metallic and polymeric materials, using the different types of IRT discussed in the previous sections. Such a graphical representation enables the potential capabilities of various inspection techniques to be mapped. It becomes clear that the size-to-depth ratio is a key factor for the recognisability of defects. Indeed, very few IRT methods can detect defects in metallic components at a depth of twice their size (Fig. 7). Laser stimulation is one of the successful exceptions, even though its application range reaches a maximum depth of just over 1 mm. Optical flash-stimulated thermography can extend the detection range to a depth of 5 mm, with a more moderate size-to-depth ratio of about 1. The enlarged inset in Fig. 7 illustrates the limited applicability of convective heat stimulation techniques, which are only effective for emerging or very shallow defects in metals. Diagrams, such as those in Figs. 7–8, are important tools to help guide industrial inspection processes towards defining quality control protocols based on the critical size and expected depth of defects.

The technical specifications of the IR camera (model, sensor type, resolution, frames per second and sensitivity) used in the literature studies reported in Table 3.

Figure 9a and Fig. 9b show graphical distributions of the different IR camera characteristics (resolution, frames per second and sensitivity) summarised in Table 3 on the basis of the IRT technique and material, respectively.

4.2 Thermography used for in-situ AM

AM process monitoring is considered a hot research topic because it might be able to ensure the detection of defects in real time during the printing process. Process monitoring allows production failures to be prevented and part quality to be ensured, thereby resulting in time, material and energy savings for the post quality control operations. Because of the complexity of an AM process, e.g. the broad temperature range, AM monitoring research is still at the early stage of development. The research so far has mainly focused on adapting or developing systems that could be used to capture features of interest for the AM process. Among these, thermography techniques are the most widely used. The design of the monitoring solution includes the identification of the features of interest, the design of the instrument that is used to perform the monitoring and its position in the AM machine.

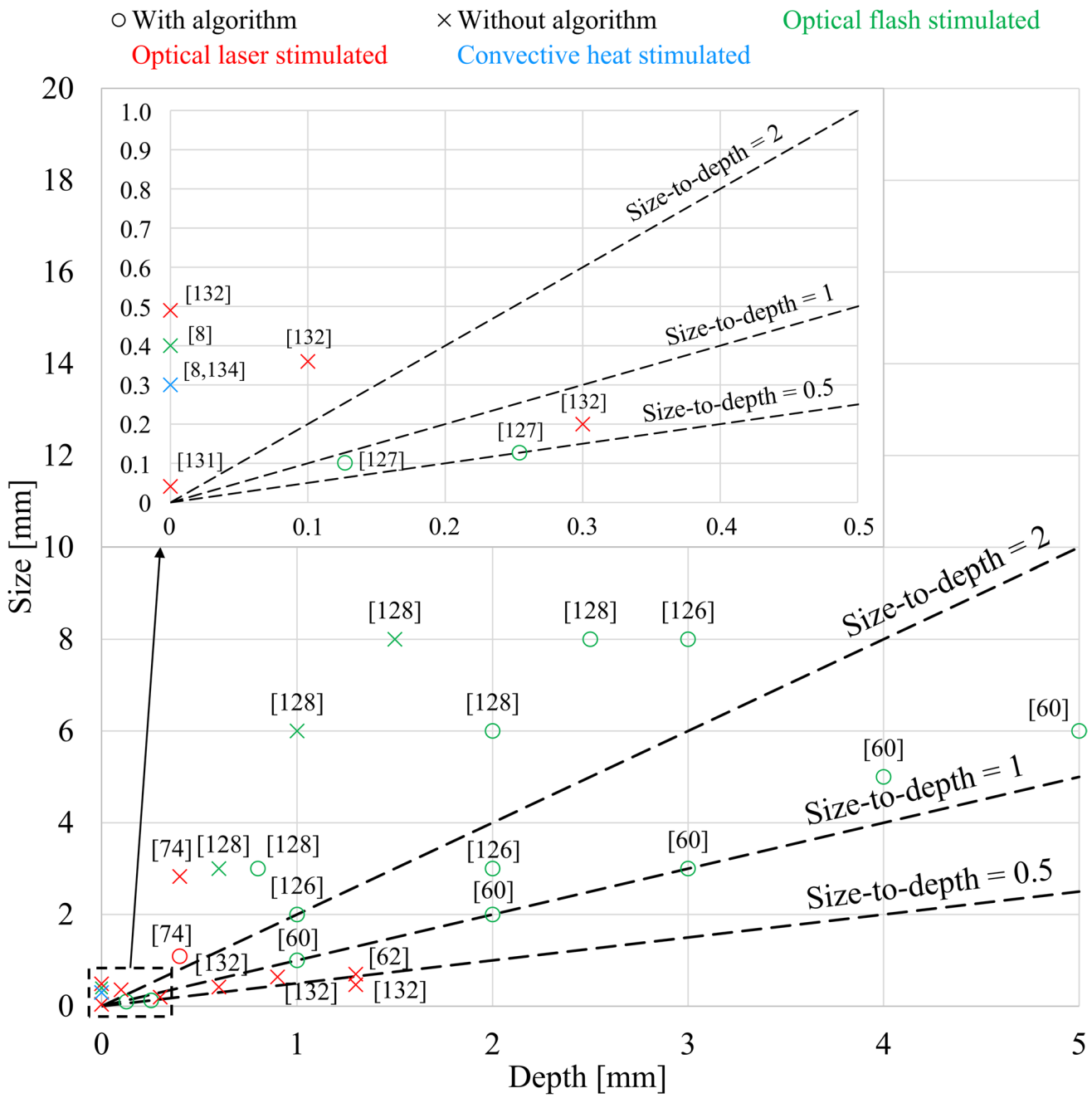

Fig. 7 Summary of the detection of small and deep defects in AM metal parts using various IRT methods

Thermal monitoring is mainly adopted in metal PBF technologies to verify whether the heat has been correctly distributed. This aspect is usually observed by measuring anomalies in the melt pool and inhomogeneity in the temperature. Pyrometers, thermocouples and thermographic cameras are the most widely used tools for the thermal in-situ monitoring of powder-bed fusion technologies [63, 151]. A thermal camera can be mounted on-axis, if the measurement is performed considering the optical path of the sources, or off-axis, if the build plane is observed [152]. In the latter case, the thermal camera can be positioned inside or outside of the build chamber and tilted relative to the build plane. Because of the simplicity of its installation, off-axis is the most widely used method with the thermal camera mounted outside the build chamber [64, 151, 153]. However, this arrangement can result in various issues, such as static (Fig. 10) or moving elements (e.g. the recoater) that could temporarily cover the field-of-view of the camera during movement [154]. Moreover, inaccuracy can be caused by the greater distance between the building plane and the

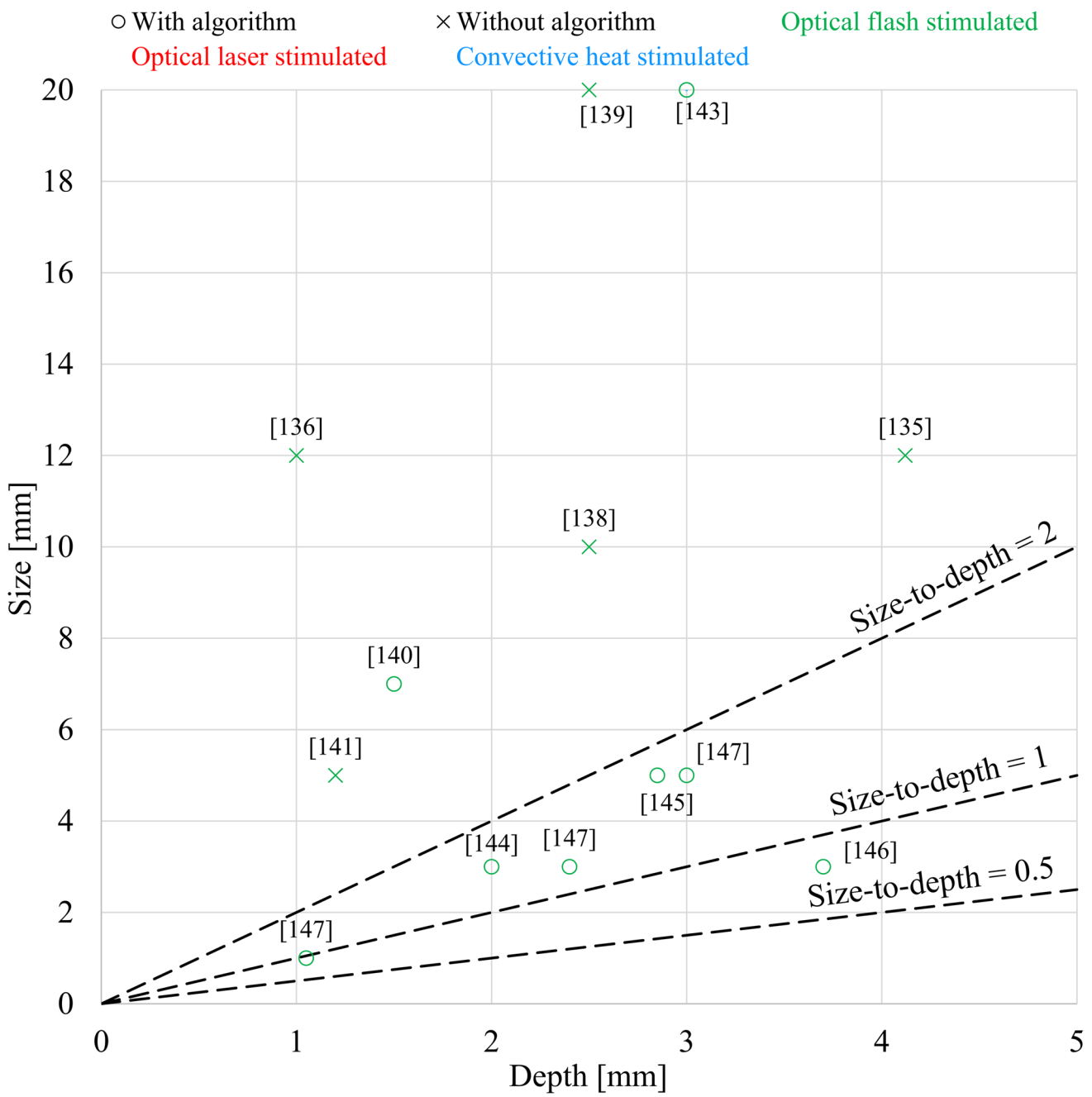

Fig. 8 Summary of the detection of small and deep defects in AM polymer parts using various IRT methods

camera and, due to the unavoidable tilting angle, different points of the same building plane result to be closer to the detector, while others are further away. At the same time, the installation of the camera inside the build chamber can be particularly challenging. In many systems, it is impossible to fit a camera, or, when it is possible, it needs to be carefully protected. Other problems are related to the measured temperature [33, 153, 155–157], which is in the form of a thermogram. Thus, thermal cameras need to be calibrated considering the effective condition of the system [154] and the material state changes during melting from powder-to-liquid-to-solid both within a layer and between all the layers [151, 158]. Furthermore, emissivity can change, depending on the surface conditions [159, 160].

The camera used in powder bed fusion with electron beam (PBF-EB) systems can be damaged by heat and metal vapour. A shutter can be used to protect the detector, that is, to both reduce excessive heat and metal vapour condensation [160]. An alternative to this solution is to unravel a thin Kapton film in front of a leaded glass, if the camera is mounted

Table 3 State of the art of the thermal imaging cameras specifications

IRT technique	Model	Type of sensor	Resolution [pixels]	FPS [Hz]	Sensitivity [mK]	Reference
Optical flash stimulated technique	FLIR X8501 sc MWIR	Indium Antimonide (InSb)	576 × 520 (299,520)	216	20	[60]
Optical flash stimulated technique	FLIR X8501 sc MWIR	Cooled detector array	1280 × 1024 (1,310,720)	181	20	[149]
Optical flash stimulated technique	FLIR A65	Focal plane array (FPA) uncooled Vanadium Oxide (VOX) microbolometer	640 × 512 (327,680)	30	50	[61, 126]
Optical flash stimulated technique	FLIR X8501 sc MWIR	Indium Antimonide (InSb)	752 × 704 (529,408)	220	< 20	[127]
Optical flash stimulated technique	FLIR X8501 sc MWIR	Indium Antimonide (InSb)	728 × 960 (698,880)	240	< 20	[127]
Optical flash stimulated technique	InfraTec ImageIR 8800	MCT	160 × 128 (20,480)	1000	< 25	[129]
Optical flash stimulated technique	InfraTec ImageIR 8300 hp	Indium Antimonide (InSb)	256 × 320 (81,920)	500	< 25	[129]
Optical flash stimulated technique	FLIR A6751 MWIR	Indium Antimonide (InSb)	640 × 512 (327,680)	125	< 18	[128]
Optical flash stimulated technique	Fluke Ti400	-	320 × 240 (76,800)	60	50	[135]
Optical flash stimulated technique	FLIR SC4000 MWIR	Indium Antimonide (InSb)	320 × 256 (81,920)	100	18	[136]
Optical flash stimulated technique	Thermosensorik CMT128	-	128 × 128 (16,384)	-	-	[137]
Optical flash stimulated technique	Fluke Ti400	-	320 × 240 (76,800)	60	50	[138]
Optical flash stimulated technique	-	-	-	-	-	[139]
Optical flash stimulated technique	FLIR T865 (focus lens 42°)	Non-cooled microbolometer, 12 µm	640 × 480 (307,200)	30	< 30	[140]
Optical flash stimulated technique	FLIR SC4000 MWIR	Indium Antimonide	320 × 256 (81,920)	60	18	[141]
Optical flash stimulated technique	Optris PI450	FPA, Non-cooled (25 µm × 25 µm	382 × 288 (110,016)	25	40	[142]
Optical flash stimulated technique	FLIR SC640	Focal Plane Arrays, Non-cooled microbolometer	640 × 480 (307,200)	30	60	[143]
Optical flash stimulated technique	FLIR GF309	Indium Antimonide cooled detector	320 × 240 (76,800)	25	25	[144]
Optical flash stimulated technique	-	-	-	3	-	[145]
Optical flash stimulated technique	InfraTec ImageIR 8800	Cooled mercury cadmium telluride focal plane array detector	640 × 512 (327,680)	233	< 25	[146]
Optical flash stimulated technique	FLIR SC7650	Indium Antimonide	320 × 256 (81,920)	100	20	[147]
Optical flash stimulated technique	-	Electrically cooled indium antimonite detector	320 × 356 (113,920)	150	30	[150]
Optical laser stimulated technique	InfraTec ImageIR 8300 hp	Indium Antimonide	640 × 512 (327,680)	355	< 25	[130]
Optical laser stimulated	InfraTec ImageIR 8800	MCT	640 × 512 (327,680)	500	< 20	[74]
Optical laser stimulated technique	FLIR X6540SC	Focal plane array	640 × 512 (327,680)	20	20	[44, 148]
Optical laser stimulated technique	FLIR X6540SC	Focal plane array	640 × 512 (327,680)	20	20	[62]

Table 3 (continued)

IRT technique	Model	Type of sensor	Resolution [pixels]	FPS [Hz]	Sensitivity [mK]	Reference
Optical laser stimulated technique	InfraTec VarioCAM head 880	Uncooled Microbolometer Focal Plane Array	640 × 480 (307,200)	60	< 20	[131]
Mechanically stimulated technique	FLIR A325SC	Uncooled Vanadium Oxide microbolometer	320 × 240 (76,800)	60	50	[133]
Convective heat stimulated technique	FLIR SC660	Focal plane array uncooled microbolometer	640 × 480 (307,200)	30	< 30	[134]
Convective heat stimulated technique	-	Electrically cooled indium antimonite detector	320 × 356 (113,920)	150	30	[150]

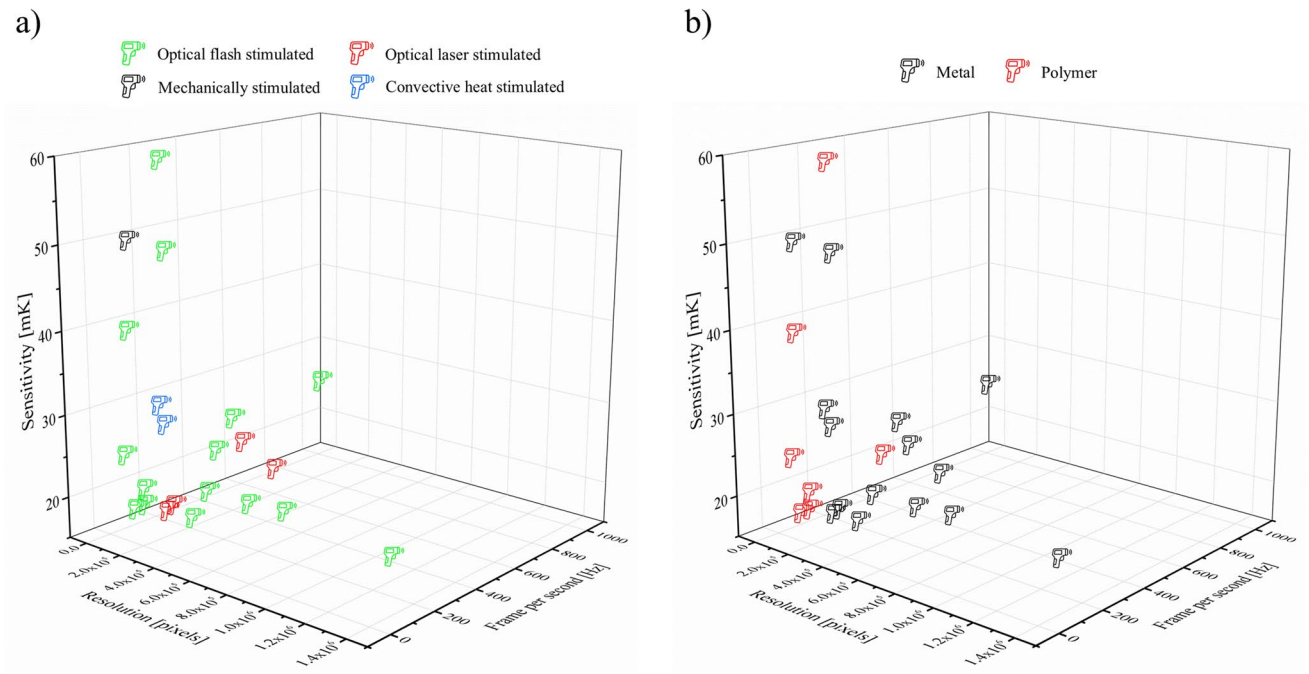

Fig. 9 Properties of the used thermal imaging cameras (FPS, resolution and sensitivity), classified according to **a**) the IRT technique, and **b**) the analysed material

outside, or in front of the lenses, if it is mounted inside. A Kapton film collects the condensing metal, thereby allowing the IR to reach the detector [161]. Rodriguez [162] proposed in-situ monitoring to measure the temperature profile of each layer and automatically detect cold zones and anomalies. The obtained data were used to adapt the process parameters and adjust the process. Price et al. [163] analysed the temperature profile in a melt pool as well as its shape and dimension. Raplee et al. [151] showed that when the temperature is inhomogeneous, it could lead to to swelling and pitting zones, which cause irregular IR emission. Cheng et al. [164] quantified the correlation between surface curvature and IR emission. Mireles et al. [64] verified artificially designed defect detection in their work, which involved performing in-situ thermography alongside ex-situ tomography.

Another PBF technology that shares similar features of interest, such as the melt pool and temperature monitoring, is PBF-LB. Kruth et al. [165] developed and patented a procedure to monitor and obtain feedback control utilising a photodiode and a complementary metal-oxide (CMOS). Craeghs et al. [166] an algorithm to monitor the melt pool, while Krauss et al. [167] demonstrated how an inadequate heat dissipation can cause flaws and pores. Bartlett et al. [72] detected, through in-situ thermography, an 82% lack-of-fusion, 100% of pores greater than 500 µm and 50% of pores smaller than 50 µm. One of the few works in which a pyrometer containing a CMOS camera had been positioned inside the build chamber was carried out by Mitchell et al. [168], who examined melt pool aspect ratios and orientations. Mohr et al. [63] utilised two different types of

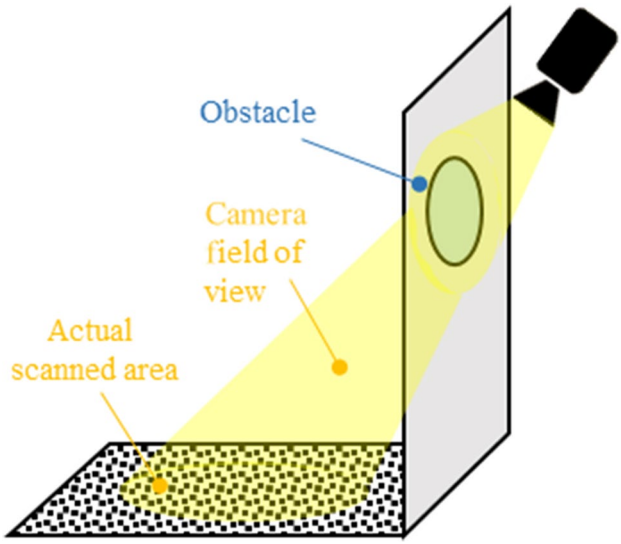

Fig. 10 The potential scanned area is reduced because of the presence of obstacles

cameras: a high-frequency IR camera and a long-time exposure camera, and they highlighted the presence of different lack-of-fusion clusters and 71% of porosities. Oster et al. [169] combined registration of in-situ thermography data with post-process XCT reference data. In this work a preprocess through a linear interpolation algorithm, a camera off-axis setup compensation and a resampling to match XCT dataset is performed. A following XCT reference data and deformation adjustment and image registration is conducted. Errico et al. [170] examined thin wall fabrication through in-situ thermography and ex-situ XCT to analyse local overheating, geometric distortions and insufficient fusion.

In-situ thermography has been also applied for Laser Metal Deposition (LMD). Among examples of such works, Mazzarisi et al. [171] assessed maximum temperature, thermal gradient and cooling rate during the deposition of nickel-based superalloy with the aim to correlate the process parameters and melt strategies with the resulting part quality. D'Accardi et al. [172] correlated thermal signatures with process parameters and considered the influence of material state, temperature, surface roughness and measurement angles to determine emissivity. The same authors [174] correlated mean and minimum apparent temperature during deposition with hardness. Altenburg et al. [175, 176, 212] compared advantage and disadvantages of the use of different wavelength in in-situ thermography summarised in tables concluding that short and mid-wave infrared are most suitable for monitoring where the emissivity variation is the main difference.

The main thermal feature of interest for AM material extrusion processes for polymers is the rate at which the filament cools down. In order to capture such information, a single thermal camera is usually positioned in such a way as to frame the nozzle and the depositing filament [177]. Seppala et al. [177] characterised the temperature profiles for MEX additive manufacturing for the polymer technology through in-situ- IR imaging.

The temperatures of the resin and of the platform are crucial for vat photopolymerization (VPP). Zhang et al. [178] considered these parameters when they developed a calibration procedure for photopolymers and for the measurement of the superficial temperature of various portions of the system. To achieve this, they chose two camera placements. Figure 11 depicts that, in position A, the camera is above the printed part, while, in position B, the camera is at the bottom and is slightly tilted.

Thermal monitoring has already been implemented in various commercial systems, because of the importance of the topic. Renishaw, for example, developed InfiniAM Spectral for PBF-LB that operates with LaserVIEW, a system composed of an IR photodiode to measure laser inputs, and with MeltVIEW, which is an in-line opto-mechanical module system [179]. Arcam AB developed a monitoring system, named LayerQam, for the PBF-EB system, which operates in IR and visible light to detect defects [180]. EOS developed a pairing of hardware and software to monitor the energy input in real time through a near-infrared camera [181] in PBF-LB processes. HP MultiJet Fusion systems (PBF-IrL/P) are equipped with a thermal camera to monitor the temperature [182].

4.3 Numerical Simulations

Numerical simulations are tools that are largely used in many fields to estimate and predict the behaviour of physical events. These tools are often valuable for evaluating and explaining phenomena that are difficult to observe at different scales. In such a context, simulations of an IRT are used to analyse the thermal behaviour of the object under analysis. IRT simulations are used, for example, to predict the thermal behaviour of flawless and defective component [57, 183]; to estimate the geometry of defects under different conditions [184]; to reduce the time for the optimisation of the IRT parameters [185, 186]; for quality control and data analysis [43]; to detect inappropriate heat flows caused by an unoptimised manufacturing process [72]; to predict manufacturing thermal efficiency [187]; and to predict the heat distribution caused by tumours [188]. The amount of scientific research on IRT simulations and their relative applications is growing, even for quality control or quality assurance (QC/QA) purposes.

IRT simulation models are based on the simulation of the heat transfer through three mechanisms: conduction, convection and radiation. Depending on the simulated system, one or more predominant mechanisms can be considered

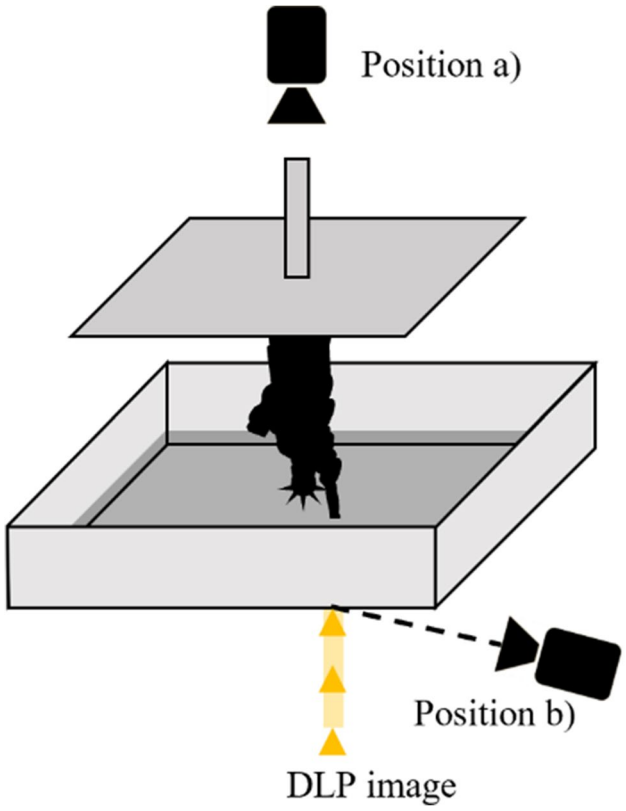

Fig. 11 Camera positioning performed by Zhang et al. Adapted from [178]

in IRT modelling. In addition, the setup of an IRT simulation involves selecting the thermography mode, the material, the component geometry and the simulation parameters. The thermography modes affect how energy is provided to the object, considering the Joule effect, radiation or friction. Depending on the form of the source, it is necessary to define how to model the resistance, current, time of exposition, emissivity, power of the source or time for the maximum SNR. The heat flows in the material are defined from the film coefficient, thermal conductivity, density and heat capacity. The simulation domain should be defined using either the full geometry or a part of it, the dimension and shape of the object and the presence, shape, dimension and position of defects. The domain can be simulated for different lengths, according to the symmetry level of the component, which can be one-dimensional, two-dimensional, or three-dimensional. The simplest models are one-dimensional. In this case, the temperature difference between a sound and defective area (ΔT) depends exclusively on the time and depth coordinates. Therefore, the contribution of lateral heat transfer is neglected.

Figure 12 shows graphically domains with one, two or three dimensions. In a one-dimensional system, the heating power against time $Q(\tau)$ is applied as a boundary condition of the domain and the heat transfer takes place along the thickness (z-axis). The only defined dimensions are the thickness of the material, z0, the dimension of the defect, z_d, and its position. From the thermal point of view, the defect is usually considered as an absolute insulator [43], and no heat transmission is therefore considered in the defect. Two-dimensional modelling is applied to an axisymmetrical system that contains, e.g., a cylindrical defect in a cylindrical volume [189]. In this case, ΔT depends on the time, defect depth and radius. Unlike the one-dimensional model, the heat $Q(\tau)$ is also transferred along the r-axis. In this case, the defect is described by the z dimensions in a similar way to the one-dimensional approach to which the radius, r_d, is integrated. In a three-dimensional simulation, all three dimensions contribute to ΔT. This is the most frequently applied method because of its level of accuracy. Since the heat transfer equations are solved along all the three dimensions, the defects can be placed in different locations of the model and the cumulative effects on the heat transfer can be analysed. Hence, the defect is represented by three dimensions: x_d, y_d, and z_d.

Among the methods used to solve the numerical model, the finite element (FE) method is the most frequently applied [138, 145, 184, 186, 190–197] because it can achieve an adequate accuracy with a limited computational cost [145]. The most frequently employed commercial solvers based on FE are COMSOL and ANSYS. In the same was as for the experiments, the results of a thermography simulation can be considered thermograms in which thermal parameters are examined, e.g. temperatures and a thermal flux. Thus, validation of the results is required to determine and tune the accuracy of the numerical results. Differentiation between the sound area and the defective area of empirical thermograms is achieved, through binarization, to obtain an effective comparison between experimental and simulation results. For this purpose, Otsu [198] proposed a binarization technique which is still one of the most effective [195]With this method, thermograms are converted into black-and-white images according to the presence or lack of a defect in the sound area.

Table 4 reviews the research on the use of simulation in thermography studies, according to the area of application, the technical simulation characteristics (dimensions of the model, the considered solver, the mode of the thermography and the material under analysis), and the experimental validation. The use of the techniques for part production is also reviewed.

As can be observed, most of the simulations involved applying a step-heating and pulsed thermography mode. PA12 Carbon Fibre fibre-reinforced polymer and aluminium alloys (CFRP) were the most commonly used materials for mechanical applications. Most studies adopted a three-dimensional approach and validated the model through

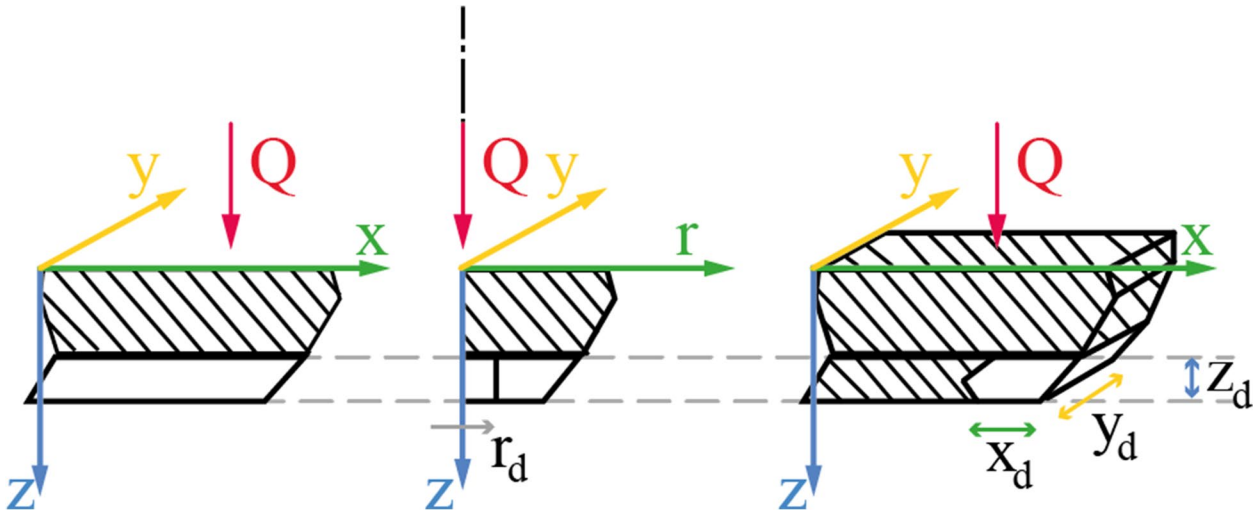

Fig. 12 Different mathematical approaches to defect modelling

experiments. Among the two-dimensional simulations, only the work in [138] was supported by experimental validation. It is worth noting that, in most cases, thermography simulation was applied to modern topics, including composites and AM. However, when AM thermography was simulated, the material properties were usually modelled as if the material had been produced using conventional manufacturing processes [199].

The main reason for using thermography simulation is to improve the QC/QA, although some of the considered works focused on the development of thermography simulations, hence improving modelling accuracy, replicating possible defect arrangements or analysing heat dissipation. In all the reviewed studies, defects were modelled as being filled with air, although Grys et al. [195] also considered iron defects. As far as validation is concerned, defects were considered for most of the reviewed works and considered as being filled with air. However, in Refs [186, 193], due to the impossibility of introducing air for lamination, Teflon was used because of its similar thermal properties.

4.4 Artificial Intelligence applied to Thermogram Analysis

As mentioned above, the analysis of the result of a thermography analysis requires experience in converting raw infrared images into significant information, especially concerning the identification of anomalies and defects. In this context, tools based on artificial intelligence, such as machine learning (ML) or deep learning, can facilitate automatic detection by automating and improving the precision of these interpretations. Zhang. et al. [207, 208] employed ML to mitigate thermographic noise during the identification of defects in metallic components. Marani et al. [209] used a deep learning technique, called convolutional neural network (CNN), to identify faults in composites, and they concluded that a two-step procedure, based on a first rapid evaluation for an initial superficial estimation and then a deeper examination for the detection of the internal pores, could be implemented.

Zhang et al. [126] proposed the use of machine learning algorithms to enhance the quality of thermal images by eliminating additive white Gaussian noise, without causing image blurring. In this way, even the smallest and deepest defects were detected. Zhang et al. [207] investigated signal separation from noise utilising machine learning techniques, namely spatial–temporal blind source separation and spatial–temporal sparse dictionary learning approaches. The efficacy of the suggested approaches was corroborated using thermography data derived from PBF-LB 316L stainless steel and Inconel 718 specimens featuring imprinted porosity defects with a diameter of 1 mm and a depth of 1 mm. Machine learning-based thermography demonstrated a superior accuracy; however, it necessitated an extended runtime. Baumgartl et al. [210] integrated CNN with thermographic pictures of H13 steel specimens produced by PBF-LB methods to identify such faults as delamination and spatter, and they achieved an accuracy of 96.80%. However, this study did not consider cracks, pores or balling. Chen et al. [211] employed passive IRT with CNN to facilitate real-time fault detection in a manufacturing process. This technology can be used to modify the processing parameters of the subsequent layer, on the basis of detection data from the current layer, and in this way closed-loop feedback on the additive manufacturing process can be achieved. Heifetz et al.

Table 4 Thermography simulation applications. N/A stands for Not available

Ref	Application and scientific fields	Part production method	Solver	Thermography mode	Material	Model	Validation
[138]	QC/QA improvement, mechanical	AM (MEX)	ANSYS	step heating	PA12	2D	Yes
[199]	thermography simulation development, mechanical	/	COMSOL	pulsed	PLA, PA12, ABS, SS316	2D	N/A
[145]	QC/QA improvement, mechanical	AM (3D printed)	Abaqus	step heating	PLA, PA12	3D	Yes
[200]	QC/QA improvement, mechanical	Composite lamination	/	pulsed	CFRP006	3D	Yes
[201]	QC/QA improvement, mechanical	Composite lamination	/	laser	CFRP	3D	Yes
[202]	QC/QA improvement, materials	spray deposition on AM part	COMSOL	pulsed	Ti64 coating on Al6061	3D	Yes
[203]	thermography simulation development, construction	/	ANSYS	lock-in	Concrete	2D	Yes
[204]	QC/QA improvement, energy	/	COMSOL	passive	wind turbine blades	3D	Yes
[205]	QC/QA improvement, mechanical	/	COMSOL	step heating	Al3003 Cu	3D	Yes
[195]	thermography simulation development, Engineering	/	/	step heating	plexiglass	2D	N/A
[194]	QC/QA improvement, Engineering	Composite lamination	COMSOL	line-scanning	CFRP	3D	Yes
[186]	QC/QA improvement, mechanical	Composite lamination	Abaqus	step heating	glass–epoxy	3D	Yes
[193]	QC/QA improvement, IT	Composite lamination	NE/Nastran	pulsed	Composite	2D/3D	Yes
[206]	thermography simulation development, eletronic	/	/	/	PCB	3D	Yes
[188]	Quality of life improvement, medical	casting in 3D printed mould	ANSYS	step heating	Silicone	3D	N/A

extracted low SNR features, related to the presence of material flaws in thermal imaging, identified by means of unsupervised machine learning algorithms [60]. They examined and confronted various algorithms and found that STBSS and STSDL were superior in the detection of defects than the other machine learning techniques they had evaluated. Nonetheless, they also found that the obtained enhancement in sensitivity implied an increase in the runtime. Oster et al. [212] compared different machine learning techniques concluding that the Random Forest method shows better performances over other techniques. The authors processed directly raw image using a combination of convolutional layers, LSTM layer and dens regression layers concluding that this technique avoids manual feature extraction resulting with increased computational complexity. Remarkable, Oster et al. [213] proposed a machine learning approach through CNN for keyhole formation prediction.

4.5 Thermography VS other Technologies in AM

The complexity of the AM process, in terms of both part design and manufacturing, has increasingly necessitated the application of advanced quality control techniques [24]. In addition to thermography, other non-destructive testing (NDT) methods have been employed. Indeed, a single NDT technique can typically only detect a limited range of defects, whereas combining multiple NDT techniques provides complementary information, thereby offering a more comprehensive evaluation of the integrity of a part [24, 214]. NDT techniques are generally categorised into imaging-based, electromagnetic, mechanical, and other specialised methods. Imaging-based NDT techniques include two-dimensional radiographic testing (RT), X-ray computed tomography (CT), synchrotron X-ray (SX) and neutron imaging (NI). Electromagnetic- based NDT techniques include potential drop testing (PD), eddy current testing (ECT) and magnetic particle testing (MPT). Mechanical NDT techniques, including ultrasonic and vibratory methods, are widely used in industry. Ultrasonic techniques consist of conventional ultrasonic testing (CUT), immersion ultrasonic testing (IUT) and phased array ultrasonic testing (PAUT). Vibration methods encompass process-compensated resonance testing (PCRT) and the resonant acoustic method (RAM). Other techniques, or even a combination of them, involve residual stress

analysis (RS), penetrant testing (PT) and visual inspection (VI) or electromagnetic-acoustic transducer ultrasonic testing (EMAT) and laser ultrasound (LU). Owing to their different natures, each NDT method presents different strengths and weaknesses, which are summarised in Table 5.

X-ray computed tomography, electromagnetic, and ultrasonic techniques are among the most frequently employed techniques in the AM field.

CT is a technique that is used to create a 3D virtual model of an object by acquiring numerous X-ray images from different rotation angles. Ultrasonic techniques use the anomalies of the transmission of acoustic emissions through an object to detect any inhomogeneity of the material. The primary advantages of ultrasonic testing are the rapid scanning speed, high resolution, effective flaw detection capabilities, and its suitability for several field applications. On the other hand, the setup and the analysis of the results are complex and require skilled personnel. In addition, the minimum detectable defect size should exceed the wavelength. Noncontact ultrasonic techniques, also known as air-coupled ultrasonic testing, use low frequencies, generally ranging from 50 to 400 kHz, which are transmitted through the air to the object that has to be inspected, without any contact. The inspection is quick [139]. However, owing to the long wavelengths, the theoretical minimum effect size is 0.85 mm at 400 kHz and 6.85 mm at 50 kHz. Eddy current testing utilises electromagnetic induction to generate a current in a conductive material. The magnitude of the induced current depends on the permeability and conductivity of the material. Therefore, any variation of such properties in a continuous material may indicate the presence of defects.

Mandache [215] analysed the anomalies and service-induced defects of NDT methods for metal-based additive manufacturing to ensure that when different operators employed the same NDT method on identical metal materials and utilised equivalent AM techniques, they would achieve consistent detection results. They found that thermography demonstrated a defect size detection capability of 10^{-2} m for surface or near-surface flaws, but ultrasonic testing (UT) and radiographic testing exhibited superior defect size detection capabilities of 10^{-3} m and 10^{-5} m, respectively, along with the ability to identify defects within the volume. Forien et al. [216] correlated a digital number (DN), generated by an in-situ pyrometer, to the presence of pores, and they verified the results through ex-situ CT on single tracks of AISI 316L produced by PBF-LB. They concluded that a higher DN corresponded to a higher probability of pores e.g. a DN > 300 indicated a probability of > 90% of the presence of pores. Ramírez et al. [217], comparing various studies, found that a defect with a size of 100 µm was detectable by means of radiographic testing, CT, and UT, although they indicated that magnetic testing was the least efficient technology, as it could only detect larger defects than 1 mm. Under the same conditions, the minimum defect size detected by means of IRT was 500 µm.

Chen et al. [218] combined several signals, such as thermal, optical, acoustic, electromagnetic and radiographic signals, to develop a closed-loop quality control specifically for wire and arc additive manufacturing (DED-Arc). Lu and Wong [219] compared acoustic emission testing and thermography in additive manufacturing processes from various works. They evaluated the advantages and disadvantages of these two NDT techniques for fault detection in AM components and their use in AM and concluded that the primary challenges in AM quality testing were the absence of real-time sensors in critical areas for process control and monitoring and the lack of closed-loop control systems.

Mireles et al. [64] compared CT and IRT on a Ti-6 Al-4 V sample produced by PBF-EB, which had been produced containing artificial defects of various shapes and dimensions, that is, from 100 µm to 2000 µm. They demonstrated that IRT could not consistently identify large pores (< 600 µm) in situ, which were instead detected post-situ through CT scans.

D'Accardi et al. [130] manufactured two samples of AISI 316L using PBF-LB with different process parameters to create squares and crosses in order to evaluate the typical defects generated by this process. The authors highlighted that thermography and eddy current testing are capable of identifying irregularly shaped defects, albeit with differing sensitivities to microstructural variations. Indeed, in thermography inspection, edge effects significantly influence the PPT method and can hinder the analysis of small specimens with defects located near the edge. The eddy current inspections were able to detect keyhole flaws more effectively, but only with the use of guided probes, although the increased contrast-to-noise ratio (CNR) [74] showed that localised common process flaws can be detected by means of both pulsed thermography and CT. However, the detection limit of the pulsed thermography approach reached a limit of 0.35 mm in size and 0.4 mm in depth. Machado et al. [139] compared the use of active thermography, eddy current testing, and air-coupled ultrasound composite samples produced by the material extrusion (MEX) additive manufacturing of polymer. The samples were produced using two different reinforced filaments made up of a polymeric matrix reinforced with 0.1 mm and 0.25 mm NiTi wires. The samples also embedded an artificial defect, positioned at the centre of the 5 mm sample to emulate delaminations of 0.1 mm and 0.5 mm. The authors found that active thermography with customised heat sources were able to detect voids and delaminations. The reinforcing fibres (NiTi wire) and their configuration were detected inside the polymeric matrix during the eddy currents inspection. Air-coupled ultrasound exhibited a superior resolution, but no NiTi wires were detected. Kolb et al. [134] used active IRT, CT and ultrasonic testing for fault detection in Inconel

Table 5 Summary of key strengths and weaknesses of NDT techniques

Type	NDT technique	Main strengths	Main weaknesses
Infrared	Infrared thermography (IRT)	- Time and cost effective - Contactless	- Difficulty in detecting micro and deep defects - Affected by emissivity and surface roughness
Imaging	Two-dimensional radiographic testing (RT)	- Possibility of detecting deep defects	- Slow and expensive - Limited part size - 2D visualisation
	X-Ray computed tomography (CT)	- Possibility of detecting deep defects - High resolution - 3D visualisation	- Slow and expensive - Limited part size - Unsuitable for online inspection
	Synchrotron X-Ray (SX)	- Possibility of detecting deep defects - Excellent resolution - 3D visualisation	
	Neutron imaging (NI)	- Possibility of detecting deep defects - High resolution - Good resolution for large samples - Suitable for light elements	
Electromagnetic	Potential drop (PD)	- Sensitive to surface cracks - Feasible at high temperatures	- Limited to conductive materials - Low penetration depth (a few mm) - Affected by surface roughness
	Eddy current testing (ECT)	- Time and cost effective - Contactless - Sensitive to small defects - Suitable for online detection	- Limited to conductive materials - Low penetration depth (a few mm) - Affected by surface roughness
	Magnetic particle testing (MPT)	- High detection sensitivity - Suitable for subsurface defects	- Limited to ferromagnetic materials - Slow and expensive - Unsuitable for online inspection
Mechanical ultrasonic	Conventional ultrasonic testing (CUT)	- Time and cost effective - Large penetration depth	- Contact required - Limited to flat surfaces - Unsuitable for complex shapes
	Immersion ultrasonic testing (IUT)	- Contactless - Time and cost effective - Large penetration depth	- Requires immersion
	Phased array ultrasonic testing (PAUT)	- Accurate spatial control - Large penetration depth - 3D visualisation	- Contact required - High cost
Mechanical vibratory	Process compensated resonance testing (PCRT)	- Fast and easy to use - Minimal setup - Automated - No size or shape limitations	- Contact required - No information about defect type or location
	Resonant acoustic method (RAM)	- Fast and easy to use - Contactless - No part size or shape limitations	- No information about defect type or location
Combined	Electromagnetic acoustic transducer ultrasound testing (EMAT)	- Contactless - Fast - Defect location and dimensions - Perfect for online inspection - Suitable for high temperatures	- Low SNR - Not effective for complex geometries - Low sensitivity for small defects
	Laser ultrasound (LU)	- Contactless - Suitable for complex geometries - Highly sensitive to small subsurface defects	- Medium penetration depth - Onerous post-processing - Unsuitable for real-time testing - Expensive equipment

Table 5 (continued)

Type	NDT technique	Main strengths	Main weaknesses
Other	Residual stress (RS)	- Large penetration depth - High resolution	- Costly and time consuming
	Penetrant testing (PT)	- Time and cost effective	- Limited to emerging defects - No information about defect type or size
	Visual inspection (VI)	- Cost-effective	- Limited to surface defects - Labour intensive

718 components produced by PBF-LB. Both CT and UT provided a minimum defect detection dimension of 300 µm. CT provided an excellent resolution, but when the sample size or the material density increased, UT was more appropriate. IRT provided a rapid and straightforward assessment of near-surface imperfections, but closed pores below the surface were not detected. The minimum size of the pores detected by means of IRT was 300 µm for an open pore defect (close to the surface). The resolution and the penetration depth of IRT were worse than in the other NDT approaches.

Sreeraj et al. [220] elaborated on prevalent concerns about AM parts, non-destructive testing (NDT) techniques for AM components, and their efficacy in addressing production and service challenges, without providing any data or specific details on the used materials or technologies.

5 Conclusions and Future Research Directions

This review highlights the growing importance of infrared thermography as a non-destructive method for the quality control of additive manufactured parts. The findings suggest that infrared thermography offers a promising, cost-effective solution for the early detection of internal defects, which is crucial to ensure product performance and reliability. An analysis of the current literature has pointed out several important conclusions:

- Effectiveness: Infrared thermography has shown a good defect detection capability in both ex-situ and in-situ applications, compared to other non-destructive techniques. The non-contact nature of this technology is particularly suitable for fast and automated inspection. However, its detection performance is highly dependent on a careful selection of the excitation method, the heating conditions, the test configuration and the post-processing algorithms.
- Limitations and challenges: Such factors as surface roughness and emissivity, as well as size and depth of the defects, can significantly affect the accuracy of thermographic measurements. In addition, the typical complex geometries of additive manufactured parts can make defect detection difficult.
- Integration with artificial intelligence and other non-destructive techniques: The ability to augment the fidelity of infrared thermography through the use of artificial intelligence tools represents a significant opportunity to improve defect detection and data interpretation. Indeed, the analysis of thermogram data can be automated and refined by integrating artificial intelligence algorithms to obtain faster and more reliable results. However, this aspect is still largely unexplored, and therefore presents considerable possibilities for better accuracy, speed, and real-time analysis. In this context, more accurate data, derived from other non-destructive testing, may be used to calibrate and tune tomography analysis. From an industrial point of view, infrared thermography may be used to complement other non-destructive testing methods and could be used for early and fast defect detection before using more expensive and time-consuming techniques, such as tomography. The review has allowed application maps to be created that could be used to select the optimal non-destructive testing technique for each application.
- Practical implications: The results strongly support the use of infrared thermography in industry and research, and they emphasise its important role in proactive defect management strategies. As the additive manufacturing industry continues to evolve, implementing robust infrared thermography systems will become essential to maintain high quality and safety standards.
- Infrared thermography maps for decision making: The proposed analysis of the state of the art has been used to develop maps that allow infrared thermography set-ups to be chosen according to the material, size, and depth of the expected defects. These maps also include information on the equipment and post-processing algorithms required for specific applications.

The interplay between infrared thermography, artificial intelligence and other non-destructive testing data is likely to define the future of quality control in this rapidly evolving field.

Acknowledgements This work has been supported by the"INTACT—Innovative additively manufactured parts inspection via non-destructive methods based on thermography and Computed Tomography"project, which was funded by the MIUR Progetti di Ricerca di Rilevante Interesse Nazionale (PRIN) Bando 2022—grant no. 2022 WA5 TJ4.

Author Contribution M.G. contributed to conceptualisation, resources, final review, paper organisation, and supervision. S.D.G. drafted the main sections on in-situ thermography, numerical simulation, and AI applied to IRT. G.R. presented defects occurring in AM and their formation mechanisms. E.T. and G.C. covered the fundamentals of thermography, industrial applications, and ex-situ thermography. L.D. provided final review and resources. E.B. contributed to the final review. L.I. supported with final review and resources. All authors have read and approved the final version of the manuscript.

Funding Open access funding provided by Politecnico di Torino within the CRUI-CARE Agreement. MIUR Progetti di Ricerca di Rilevante Interesse Nazionale (PRIN) Bando 2022, 2022 WA5 TJ4, 2022 WA5 TJ4, 2022 WA5 TJ4

Data Availability No datasets were generated or analysed during the current study.

Declarations

Competing interests The authors declare no competing interests.

References

1. Galati, M., Iuliano, L.: A literature review of powder-based electron beam melting focusing on numerical simulations. Addit. Manuf. **19**, 1–20 (2018). https://doi.org/10.1016/j.addma.2017.11.001
2. Ford, S., Despeisse, M.: Additive manufacturing and sustainability: an exploratory study of the advantages and challenges. J. Clean. Prod. **137**, 1573–1587 (2016). https://doi.org/10.1016/j.jclepro.2016.04.150
3. Lunetto, V., Galati, M., Settineri, L., Iuliano, L.: Sustainability in the manufacturing of composite materials: A literature review and directions for future research. J. Manuf. Process. **85**, 858–874 (2023). https://doi.org/10.1016/j.jmapro.2022.12.020
4. Calignano, F., Galati, M., Iuliano, L., Minetola, P.: Design of additively manufactured structures for biomedical applications: a review of the additive manufacturing processes applied to the biomedical sector. J Healthc Eng **2019**, 1–6 (2019). https://doi.org/10.1155/2019/9748212
5. Galati, M., Defanti, S.: Additive manufacturing of locally weakened parts to obtain a designed fracture. Met. Mater. Int. **30**, 323–332 (2024). https://doi.org/10.1007/s12540-023-01506-7
6. Chen, Z., Han, C., Gao, M., Kandukuri, S.Y., Zhou, K.: A review on qualification and certification for metal additive manufacturing. Virtual Phys Prototyp **17**, 382–405 (2022). https://doi.org/10.1080/17452759.2021.2018938
7. Seifi, M., Salem, A., Beuth, J., Harrysson, O., Lewandowski, J.J.: Overview of materials qualification needs for metal additive manufacturing. JOM **68**, 747–764 (2016). https://doi.org/10.1007/s11837-015-1810-0
8. ASTM International, ISO/ASTMTR52905 - Additive Manufacturing of Metals - Nondestructive Testing and Evaluation - Defect Detection in Parts, ASTM International100 Barr Harbor Drive, PO Box C700, West Conshohocken, PA 19428–2959, 2023. https://doi.org/10.1520/ISO/ASTMTR52905-EB.
9. ASTM International, E3166–20 Standard Guide for Nondestructive Examination of Metal Additively Manufactured Aerospace Parts After Build, (2020). https://doi.org/10.1520/E3166-20.
10. Zhu, Y., Wu, Z., Hartley, W.D., Sietins, J.M., Williams, C.B., Yu, H.Z.: Unraveling pore evolution in post-processing of binder jetting materials: X-ray computed tomography, computer vision, and machine learning. Addit. Manuf. **34**, 101183 (2020). https://doi.org/10.1016/j.addma.2020.101183
11. Snow, Z., Nassar, A.R., Reutzel, E.W.: Invited Review Article: Review of the formation and impact of flaws in powder bed fusion additive manufacturing. Addit. Manuf. **36**, 101457 (2020). https://doi.org/10.1016/j.addma.2020.101457
12. Gui, Y., Aoyagi, K., Chiba, A.: Development of macro-defect-free PBF-EB-processed Ti–6Al–4V alloys with superior plasticity using PREP-synthesized powder and machine learning-assisted process optimization. Mater. Sci. Eng., A **864**, 144595 (2023). https://doi.org/10.1016/j.msea.2023.144595
13. Charalampous, P., Kostavelis, I., Tzovaras, D.: Non-destructive quality control methods in additive manufacturing: a survey. Rapid Prototyp J **26**, 777–790 (2020). https://doi.org/10.1108/RPJ-08-2019-0224
14. Du, C., Zhao, Y., Jiang, J., Wang, Q., Wang, H., Li, N., Sun, J.: Pore defects in Laser Powder Bed Fusion: Formation mechanism, control method, and perspectives. J. Alloys Compd. **944**, 169215 (2023). https://doi.org/10.1016/j.jallcom.2023.169215
15. Liu, T., Guessasma, S., Zhu, J., Zhang, W., Nouri, H., Belhabib, S.: Microstructural defects induced by stereolithography and related compressive behaviour of polymers. J. Mater. Process. Technol. **251**, 37–46 (2018). https://doi.org/10.1016/j.jmatprotec.2017.08.014
16. Zhang, K., Meng, Q., Qu, Z., He, R.: A review of defects in vat photopolymerization additive-manufactured ceramics: Characterization, control, and challenges. J. Eur. Ceram. Soc. **44**, 1361–1384 (2024). https://doi.org/10.1016/j.jeurceramsoc.2023.10.067
17. Al-Maharma, A.Y., Patil, S.P., Markert, B.: Effects of porosity on the mechanical properties of additively manufactured components: a critical review. Mater Res Express **7**, 122001 (2020). https://doi.org/10.1088/2053-1591/abcc5d
18. Yang, X., Li, Y., Li, B.: Formation mechanisms of lack of fusion and keyhole-induced pore defects in laser powder bed fusion process: A numerical study. Int. J. Therm. Sci. **188**, 108221 (2023). https://doi.org/10.1016/j.ijthermalsci.2023.108221
19. Zhao, R., Shmatok, A., Fischer, R., Prorok, B.C.: Investigation of Causal Relationships between Printing Parameters, Pore Properties and Porosity in Laser Powder Bed Fusion. Metals (Basel) **13**, 330 (2023). https://doi.org/10.3390/met13020330
20. Palm, M.S., Diepold, B., Neumeier, S., Hoeppel, H.W., Goeken, M., Zaeh, M.F.: Detection and effects of lack of fusion defects in Hastelloy X manufactured by laser powder bed fusion. Mater. Des. **230**, 111941 (2023). https://doi.org/10.1016/j.matdes.2023.111941
21. Papazetis, G., Vosniakos, G.-C.: Mapping of deposition-stable and defect-free additive manufacturing via material extrusion

from minimal experiments. Int. J. Adv. Manuf. Technol. **100**, 2207–2219 (2019). https://doi.org/10.1007/s00170-018-2820-1
22. Wang, W., Zhang, Y., Yue, C., Kong, X., Hao, Z., Wang, T., Li, T.: Processing defect, microstructure evolution and mechanical properties of laser powder bed fusion Al-12Si alloys. J. Market. Res. **26**, 681–696 (2023). https://doi.org/10.1016/j.jmrt.2023.07.231
23. M. Neikter, F. Forsberg, M.-L. Antti, P. Åkerfeldt, S. Larsson, P. Jonsén, G. Puyoo, Defect characterization of electron beam melted Ti-6Al-4V and Alloy 718 with X-ray microtomography, Aeronautics and Aerospace Open Access Journal 2 (2018). https://doi.org/10.15406/aaoaj.2018.02.00044.
24. Rao, J., Leong Sing, S., Liu, P., Wang, J., Sohn, H.: Non-destructive testing of metal-based additively manufactured parts and processes: a review. Virtual Phys. Prototyp. **18**, e2266658 (2023). https://doi.org/10.1080/17452759.2023.2266658
25. Nadimpalli, V.K., Karthik, G.M., Janakiram, G.D., Nagy, P.B.: Monitoring and repair of defects in ultrasonic additive manufacturing. Int. J. Adv. Manuf. Technol. **108**, 1793–1810 (2020). https://doi.org/10.1007/s00170-020-05457-w
26. Bae, C.-J., Halloran, J.W.: Influence of residual monomer on cracking in ceramics fabricated by stereolithography. Int. J. Appl. Ceram. Technol. **8**, 1289–1295 (2011). https://doi.org/10.1111/j.1744-7402.2010.02578.x
27. Kouraytem, N., Chiang, P.-J., Jiang, R., Kantzos, C., Pauza, J., Cunningham, R., Wu, Z., Tang, G., Parab, N., Zhao, C., Fezzaa, K., Sun, T., Rollett, A.D.: Solidification crack propagation and morphology dependence on processing parameters in AA6061 from ultra-high-speed x-ray visualization. Addit. Manuf. **42**, 101959 (2021). https://doi.org/10.1016/j.addma.2021.101959
28. Bagavathiappan, S., Lahiri, B.B., Saravanan, T., Philip, J., Jayakumar, T.: Infrared thermography for condition monitoring – A review. Infrared Phys. Technol. **60**, 35–55 (2013). https://doi.org/10.1016/j.infrared.2013.03.006
29. B. Wiecek, Review on thermal image processing for passive and active thermography, in: 2005 IEEE Engineering in Medicine and Biology 27th Annual Conference, IEEE, 2005: pp. 686–689. https://doi.org/10.1109/IEMBS.2005.1616506
30. Ibarra-Castanedo, C., Tarpani, J.R., Maldague, X.P.V.: Nondestructive testing with thermography. Eur. J. Phys. **34**, S91–S109 (2013). https://doi.org/10.1088/0143-0807/34/6/S91
31. Yang, R., He, Y.: Optically and non-optically excited thermography for composites: A review. Infrared Phys. Technol. **75**, 26–50 (2016). https://doi.org/10.1016/j.infrared.2015.12.026
32. Modest, M.F.: Radiative heat transfer. Elsevier (2013). https://doi.org/10.1016/C2010-0-65874-3
33. Usamentiaga, R., Venegas, P., Guerediaga, J., Vega, L., Molleda, J., Bulnes, F.: Infrared thermography for temperature measurement and non-destructive testing. Sensors **14**, 12305–12348 (2014). https://doi.org/10.3390/s140712305
34. Arora, V., Mulaveesala, R., Bhambhu, S.K., Sharma, S., Singh, I., Das, P., Sharma, A., Dua, G.: Thermal non-destructive testing and evaluation for inspection of carbon fibre-reinforced polymers. Insight - Non-Destruct Testing Condition Monit. **66**, 409–414 (2024). https://doi.org/10.1784/insi.2024.66.7.409
35. S.I. Melnyk, I.G. Tuluzov, A.S. Melnyk, Method of remote dynamic thermographic testing of wind turbine blades, in: Proceedings of the 2014 International Conference on Quantitative InfraRed Thermography, QIRT Council, 2014. https://doi.org/10.21611/qirt.2014.037.
36. Vavilov, V., Grinzato, E., Bison, P.G., Marinetti, S., Bales, M.J.: Surface transient temperature inversion for hidden corrosion characterisation: theory and applications. Int. J. Heat Mass Transf. **39**, 355–371 (1996). https://doi.org/10.1016/0017-9310(95)00126-T
37. Harizi, W., Chaki, S., Bourse, G., Ourak, M.: Mechanical damage assessment of Glass Fiber-Reinforced Polymer composites using passive infrared thermography. Compos. B Eng. **59**, 74–79 (2014). https://doi.org/10.1016/j.compositesb.2013.11.021
38. Lahiri, B.B., Bagavathiappan, S., Jayakumar, T., Philip, J.: Medical applications of infrared thermography: A review. Infrared Phys. Technol. **55**, 221–235 (2012). https://doi.org/10.1016/j.infrared.2012.03.007
39. Vavilov, V.P., Burleigh, D.D.: Review of pulsed thermal NDT: Physical principles, theory and data processing. NDT and E Int. **73**, 28–52 (2015). https://doi.org/10.1016/j.ndteint.2015.03.003
40. He, Y., Yang, R.: Eddy Current Volume Heating Thermography and Phase Analysis for Imaging Characterization of Interface Delamination in CFRP. IEEE Trans Industr Inform **11**, 1287–1297 (2015). https://doi.org/10.1109/TII.2015.2479856
41. Zhang, H., Yang, R., He, Y., Foudazi, A., Cheng, L., Tian, G.: A review of microwave thermography nondestructive testing and evaluation. Sensors **17**, 1123 (2017). https://doi.org/10.3390/s17051123
42. Y. He, B. Gao, A. Sophian, R. Yang, Transient electromagnetic-thermal nondestructive testing: pulsed eddy current and transient eddy current thermography, 2017.
43. Vavilov, V., Burleigh, D.: Infrared thermography and thermal nondestructive testing, springer international publishing. Cham (2020). https://doi.org/10.1007/978-3-030-48002-8
44. Cerniglia, D., Montinaro, N.: Defect detection in additively manufactured components: laser ultrasound and laser thermography comparison. Procedia Structural Integrity **8**, 154–162 (2018). https://doi.org/10.1016/j.prostr.2017.12.016
45. Dong, L., Wang, B., Wang, H., Xiang, M., Chen, X., Ma, G., Di, Y., Guo, W., Kang, J., Zhou, X.: Effects of crack surface roughness on crack heat generation characteristics of ultrasonic infrared thermography. Infrared Phys. Technol. **106**, 103262 (2020). https://doi.org/10.1016/j.infrared.2020.103262
46. Sakagami, T., Ogura, K.: New flaw inspection technique based on infrared thermal images under joule effect heating. Int. J Ser. A, Mech. Mater. Eng. **37**, 380–388 (1994). https://doi.org/10.1299/jsmea1993.37.4_380
47. Y. He, M. Pan, F. Luo, Defect characterisation based on heat diffusion using induction thermography testing. Rev. Sci. Instruments 83 (2012). https://doi.org/10.1063/1.4756211.
48. Lahiri, B.B., Bagavathiappan, S., Reshmi, P.R., Philip, J., Jayakumar, T., Raj, B.: Quantification of defects in composites and rubber materials using active thermography. Infrared Phys. Technol. **55**, 191–199 (2012). https://doi.org/10.1016/j.infrared.2012.01.001
49. Maierhofer, C., Brink, A., Röllig, M., Wiggenhauser, H.: Transient thermography for structural investigation of concrete and composites in the near surface region. Infrared Phys. Technol. **43**, 271–278 (2002). https://doi.org/10.1016/S1350-4495(02)00151-2
50. Sakagami, T., Kubo, S.: Applications of pulse heating thermography and lock-in thermography to quantitative nondestructive evaluations. Infrared Phys. Technol. **43**, 211–218 (2002). https://doi.org/10.1016/S1350-4495(02)00141-X
51. Lu, X., Tian, G., Wu, J., Gao, B., Tian, P.: Pulsed air-flow thermography for natural crack detection and evaluation. IEEE Sens. J. **20**, 8091–8097 (2020). https://doi.org/10.1109/JSEN.2020.2982556
52. Dorafshan, S., Maguire, M., Collins, W.: Infrared thermography for weld inspection: feasibility and application. Infrastructures (Basel) **3**, 45 (2018). https://doi.org/10.3390/infrastructures3040045
53. Sagarduy-Marcos, D., Batsale, J.C., Rodríguez-Aseguinolaza, J.: Quantitative optimization analysis of lock-in infrared thermography for characterizing delaminations. Int. J. Heat. Mass. Transf. **231**, 125748 (2024). https://doi.org/10.1016/j.ijheatmasstransfer.2024.125748

54. Hung, Y.Y., Chen, Y.S., Ng, S.P., Liu, L., Huang, Y.H., Luk, B.L., Ip, R.W.L., Wu, C.M.L., Chung, P.S.: Review and comparison of shearography and active thermography for nondestructive evaluation. Mater. Sci. Eng. R. Rep. **64**, 73–112 (2009). https://doi.org/10.1016/j.mser.2008.11.001
55. Doshvarpassand, S., Wu, C., Wang, X.: An overview of corrosion defect characterization using active infrared thermography. Infrared Phys. Technol. **96**, 366–389 (2019). https://doi.org/10.1016/j.infrared.2018.12.006
56. Gryś, S., Minkina, W.: Noninvasive methods of active thermographic investigation: short overview of theoretical foundations with an example of application. Energies (Basel) **15**, 4865 (2022). https://doi.org/10.3390/en15134865
57. Pawar, S.S., Vavilov, V.P.: Applying the heat conduction-based 3D normalization and thermal tomography to pulsed infrared thermography for defect characterization in composite materials. Int. J. Heat Mass Transf. **94**, 56–65 (2016). https://doi.org/10.1016/j.ijheatmasstransfer.2015.11.018
58. Ibarra-Castanedo, C., Piau, J.-M., Guilbert, S., Avdelidis, N.P., Genest, M., Bendada, A., Maldague, X.P.V.: Comparative study of active thermography techniques for the nondestructive evaluation of honeycomb structures. Res. Nondestr. Eval. **20**, 1–31 (2009). https://doi.org/10.1080/09349840802366617
59. Ciampa, F., Mahmoodi, P., Pinto, F., Meo, M.: Recent advances in active infrared thermography for non-destructive testing of aerospace components. Sensors **18**, 609 (2018). https://doi.org/10.3390/s18020609
60. Heifetz, A., Zhang, X., Saniie, J., Cleary, W.: Detection of defects in additively manufactured metallic materials with machine learning of pulsed thermography images, Argonne. IL (United States) (2020). https://doi.org/10.2172/1673390
61. Performance of Compact Pulsed Thermal Imaging System for In-Service Applications, n.d. www.anl.gov.
62. Montinaro, N., Cerniglia, D., Pitarresi, G.: Defect detection in additively manufactured titanium prosthesis by flying laser scanning thermography. Procedia Structural Integrity **12**, 165–172 (2018). https://doi.org/10.1016/j.prostr.2018.11.098
63. Mohr, G., Altenburg, S.J., Ulbricht, A., Heinrich, P., Baum, D., Maierhofer, C., Hilgenberg, K.: In-situ defect detection in laser powder bed fusion by using thermography and optical tomography—comparison to computed tomography. Metals (Basel) **10**, 103 (2020). https://doi.org/10.3390/met10010103
64. Mireles, J., Ridwan, S., Morton, P.A., Hinojos, A., Wicker, R.B.: Analysis and correction of defects within parts fabricated using powder bed fusion technology. Surf Topogr **3**, 034002 (2015). https://doi.org/10.1088/2051-672X/3/3/034002
65. Boone, N., Zhu, C., Smith, C., Todd, I., Willmott, J.R.: Thermal near infrared monitoring system for electron beam melting with emissivity tracking. Addit. Manuf. **22**, 601–605 (2018). https://doi.org/10.1016/j.addma.2018.06.004
66. He, Y., Deng, B., Wang, H., Cheng, L., Zhou, K., Cai, S., Ciampa, F.: Infrared machine vision and infrared thermography with deep learning: A review. Infrared Phys. Technol. **116**, 103754 (2021). https://doi.org/10.1016/j.infrared.2021.103754
67. Fu, Y., Downey, A.R.J., Yuan, L., Zhang, T., Pratt, A., Balogun, Y.: Machine learning algorithms for defect detection in metal laser-based additive manufacturing: A review. J. Manuf. Process. **75**, 693–710 (2022). https://doi.org/10.1016/j.jmapro.2021.12.061
68. Alfredo Osornio-Rios, R., Antonino-Daviu, J.A., de Jesus Romero-Troncoso, R.: Recent industrial applications of infrared thermography: a review. IEEE Trans Industr Inform **15**, 615–625 (2019). https://doi.org/10.1109/TII.2018.2884738
69. Gonzalez-Hernandez, J.-L., Recinella, A.N., Kandlikar, S.G., Dabydeen, D., Medeiros, L., Phatak, P.: Technology, application and potential of dynamic breast thermography for the detection of breast cancer. Int. J. Heat Mass Transf. **131**, 558–573 (2019). https://doi.org/10.1016/j.ijheatmasstransfer.2018.11.089
70. Scalbi, A., Olmi, R., Inglese, G.: Evaluation of fractures in a concrete slab by means of laser-spot thermography. Int. J. Heat Mass Transf. **141**, 282–293 (2019). https://doi.org/10.1016/j.ijheatmasstransfer.2019.06.082
71. M. Galati, Electron beam melting process, in: Addit Manuf, Elsevier, 2021: pp. 277–301. https://doi.org/10.1016/B978-0-12-818411-0.00014-8.
72. Bartlett, J.L., Heim, F.M., Murty, Y.V., Li, X.: In situ defect detection in selective laser melting via full-field infrared thermography. Addit. Manuf. **24**, 595–605 (2018). https://doi.org/10.1016/j.addma.2018.10.045
73. N.J. Wallace, Active Thermography for Additive Manufacturing Processes, 2021. https://scholarsarchive.byu.edu/etd/9646.
74. D'Accardi, E., Ulbricht, A., Krankenhagen, R., Palumbo, D., Galietti, U.: Capability of active thermography to detect and localize pores in Metal Additive Manufacturing materials. IOP Conf Ser Mater Sci Eng **1038**, 012018 (2021). https://doi.org/10.1088/1757-899X/1038/1/012018
75. Vavilov, V.P.: Pulsed thermal NDT of materials: back to the basics. Nondestructive Testing and Evaluation **22**, 177–197 (2007). https://doi.org/10.1080/10589750701448407
76. S.M. Shepard, Advances in pulsed thermography, in: A.E. Rozlosnik, R.B. Dinwiddie (Eds.), 2001: pp. 511–515. https://doi.org/10.1117/12.421032.
77. Li, B., Ye, L., Li, E., Shou, D., Li, Z., Chang, L.: Gapped smoothing algorithm applied to defect identification using pulsed thermography. Nondestruct. Testing Eval. **30**, 171–195 (2015). https://doi.org/10.1080/10589759.2015.1029477
78. A. Degiovanni, A.-S. Lamine, A.-S. Houlbert, D. Maillet, Identification of Subsurface Defects by a Thermal Method Using a Sensibility Analysis, in: Developments in the Science and Technology of Composite Materials, Springer Netherlands, Dordrecht, 1990: pp. 691–696. https://doi.org/10.1007/978-94-009-0787-4_96.
79. Aamodt, L.C., Spicer, J.W.M., Murphy, J.C.: Analysis of characteristic thermal transit times for time-resolved infrared radiometry studies of multilayered coatings. J. Appl. Phys. **68**, 6087–6098 (1990). https://doi.org/10.1063/1.346897
80. J.-C. Krapez, D. Balageas, Early detection of thermal contrast in pulsed stimulated infrared thermography, in: Proceedings of the 1994 International Conference on Quantitative InfraRed Thermography, QIRT Council, 1994. https://doi.org/10.21611/qirt.1994.039.
81. M. Denis, Thermal Quadrupoles : Solving the Heat Equation Through Integral Transforms, 2000.
82. Maldague, X., Marinetti, S.: Pulse phase infrared thermography. J. Appl. Phys. **79**, 2694–2698 (1996). https://doi.org/10.1063/1.362662
83. V.P. Vavilov, S. Marinetti, E.G. Grinzato, P.G. Bison, Thermal tomography characterization and pulse-phase thermography of impact damage in CFRP, or why end users are still reluctant about practical use of transient IR thermography, in: J.R. Snell, Jr., R.N. Wurzbach (Eds.), 1998: pp. 275–281. https://doi.org/10.1117/12.304737.
84. D'Accardi, E., Palano, F., Tamborrino, R., Palumbo, D., Tatì, A., Terzi, R., Galietti, U.: Pulsed phase thermography approach for the characterization of delaminations in CFRP and comparison to phased array ultrasonic testing. J. Nondestr. Eval. **38**, 20 (2019). https://doi.org/10.1007/s10921-019-0559-8
85. Rajic, N.: Principal component thermography for flaw contrast enhancement and flaw depth characterisation in composite structures. Compos. Struct. **58**, 521–528 (2002). https://doi.org/10.1016/S0263-8223(02)00161-7

86. F.J. Madruga, C. Ibarra-Castanedo, O.M. Conde, X.P. Maldague, J.M. López-Higuera, Enhanced contrast detection of subsurface defects by pulsed infrared thermography based on the fourth order statistic moment, kurtosis, in: D.D. Burleigh, R.B. Dinwiddie (Eds.), Thermosense XXXI, SPIE, 2009: p. 72990U. https://doi.org/10.1117/12.818684.
87. Vavilov, V.P.: Dynamic thermal tomography: Recent improvements and applications. NDT and E Int. **71**, 23–32 (2015). https://doi.org/10.1016/j.ndteint.2014.09.010
88. M. Bajorek, A. Nowakowski, Analysis of the possibility of defect determination using cold excitation in thermal tomography, in: Proceedings of the 2010 International Conference on Quantitative InfraRed Thermography, QIRT Council, 2010. https://doi.org/10.21611/qirt.2010.010.
89. H.I. Ringermacher, Thermal Imaging at General Electric, in: AIP Conf Proc, AIP, 2006: pp. 523–528. https://doi.org/10.1063/1.2184572.
90. Ciliberto, A., Cavaccini, G., Salvetti, O., Chimenti, M., Azzarelli, L., Bison, P.G., Marinetti, S., Freda, A., Grinzato, E.: Porosity detection in composite aeronautical structures. Infrared Phys. Technol. **43**, 139–143 (2002). https://doi.org/10.1016/S1350-4495(02)00132-9
91. Usamentiaga, R., Venegas, P., Guerediaga, J., Vega, L., López, I.: Automatic detection of impact damage in carbon fiber composites using active thermography. Infrared Phys. Technol. **58**, 36–46 (2013). https://doi.org/10.1016/j.infrared.2013.01.004
92. H. Elwarfalli, D. Papazoglou, D. Erdahl, A. Doll, J. Speltz, In Situ Process Monitoring for Laser-Powder Bed Fusion using Convolutional Neural Networks and Infrared Tomography, in: 2019 IEEE National Aerospace and Electronics Conference (NAECON), IEEE, 2019: pp. 323–327. https://doi.org/10.1109/NAECON46414.2019.9058251
93. Inês Silva, M., Malitckii, E., Santos, T.G., Vilaça, P.: Review of conventional and advanced non-destructive testing techniques for detection and characterization of small-scale defects. Prog Mater Sci **138**, 101155 (2023). https://doi.org/10.1016/j.pmatsci.2023.101155
94. Vadivambal, R., Jayas, D.S.: Applications of thermal imaging in agriculture and food industry—a review. Food Bioproc Tech **4**, 186–199 (2011). https://doi.org/10.1007/s11947-010-0333-5
95. A. Massaro, A. Panarese, A. Galiano, Infrared Thermography applied on Fresh Food Monitoring in Automated Alerting Systems, in: 2020 IEEE International Workshop on Metrology for Industry 4.0 & IoT, IEEE, 2020: pp. 554–558. https://doi.org/10.1109/MetroInd4.0IoT48571.2020.9138207
96. P. Meinlschmidt, V. Maergner, Detection of foreign substances in food using thermography, in: X.P. Maldague, A.E. Rozlosnik (Eds.), 2002: pp. 565–571. https://doi.org/10.1117/12.459608.
97. Jones, C.H.: Medical thermography. IEE Proc A Phys Sci, Meas Instrum, Manag Educ, Reviews **134**, 225 (1987). https://doi.org/10.1049/ip-a-1.1987.0030
98. Kozhevnikova, I.S., Pankov, M.N., Gribanov, A.V., Startseva, L.F., Ermoshina, N.A.: The use of infrared thermography in modern medicine (Literature Review). Ekologiya Cheloveka (Human Ecology) **24**, 39–46 (2017). https://doi.org/10.33396/1728-0869-2017-2-39-46
99. Büyüköztürk, O.: Imaging of concrete structures. NDT and E Int. **31**, 233–243 (1998). https://doi.org/10.1016/S0963-8695(98)00012-7
100. Grinzato, E.: Infrared thermography recent advances and future trends. Bentham Science Publishers (2012). https://doi.org/10.2174/97816080514341120101
101. Maldaque, X.P.V.: Infrared Methodology and Technology, CRC Press. London (2023). https://doi.org/10.1201/9781003420200
102. C. Meola, S. Boccardi, G.M. Carlomagno, Infrared Thermography in the Evaluation of Aerospace Composite Materials, 2015. https://www.researchgate.net/publication/303987507.
103. Deane, S., Avdelidis, N.P., Ibarra-Castanedo, C., Zhang, H., Yazdani Nezhad, H., Williamson, A.A., Mackley, T., Davis, M.J., Maldague, X., Tsourdos, A.: Application of NDT thermographic imaging of aerospace structures. Infrared Phys Technol **97**, 456–466 (2019). https://doi.org/10.1016/j.infrared.2019.02.002
104. Pearlman, M., Lupercio, A., Rektor, A., Lamb, J., Fleming, A., Jaques, B., Subbaraman, H., Kandandai, N.: Infrared thermography method to detect cracking of nuclear fuels in real-time. Nucl. Eng. Des. **405**, 112196 (2023). https://doi.org/10.1016/j.nucengdes.2023.112196
105. N.I. Bazaleev, V.V. Lytvynenko, Application of active thermography for defectoscopy of technological equipment on objects of the nuclear power plants, Problems of Atomic Science and Technology (2019) 179–185. https://doi.org/10.46813/2019-123-179.
106. R.D. Lucier, J.C. Bognet, Thermography In Commercial Nuclear Power Stations Applications, Limitations, And Realities, in: G.B. McIntosh (Ed.), 1989: p. 56. https://doi.org/10.1117/12.953386.
107. Nazmul Huda, A.S., Taib, S., Jadin, M.S., Ishak, D.: A semi-automatic approach for thermographic inspection of electrical installations within buildings. Energy Build **55**, 585–591 (2012). https://doi.org/10.1016/j.enbuild.2012.09.014
108. Jadin, M.S., Taib, S.: Recent progress in diagnosing the reliability of electrical equipment by using infrared thermography. Infrared Phys. Technol. **55**, 236–245 (2012). https://doi.org/10.1016/j.infrared.2012.03.002
109. M. Weiping, C. Fangxiao, S. Ying, X. Chungui, A. Ming, Fault Diagnosis On Power Transformers Using Non-electric Method, in: 2006 IEEE International Symposium on Industrial Electronics, IEEE, 2006: pp. 1769–1773. https://doi.org/10.1109/ISIE.2006.295839
110. Kim, H.-J., Lee, J.-H., Baek, D.-H., Lee, J.-K.: A study on thermal performance of batteries using thermal imaging and infrared radiation. J. Ind. Eng. Chem. **45**, 360–365 (2017). https://doi.org/10.1016/j.jiec.2016.10.003
111. Y.-C. Chou, L. Yao, Automatic Diagnostic System of Electrical Equipment Using Infrared Thermography, in: 2009 International Conference of Soft Computing and Pattern Recognition, IEEE, 2009: pp. 155–160. https://doi.org/10.1109/SoCPaR.2009.41
112. Stipetic, S., Kovacic, M., Hanic, Z., Vrazic, M.: Measurement of excitation winding temperature on synchronous generator in rotation using infrared thermography. IEEE Trans. Industr. Electron. **59**, 2288–2298 (2012). https://doi.org/10.1109/TIE.2011.2158047
113. Arrazola, P.J., Arriola, I., Davies, M.A.: Analysis of the influence of tool type, coatings, and machinability on the thermal fields in orthogonal machining of AISI 4140 steels. CIRP Ann. **58**, 85–88 (2009). https://doi.org/10.1016/j.cirp.2009.03.085
114. Armendia, M., Garay, A., Villar, A., Davies, M.A., Arrazola, P.J.: High bandwidth temperature measurement in interrupted cutting of difficult to machine materials. CIRP Ann. **59**, 97–100 (2010). https://doi.org/10.1016/j.cirp.2010.03.059
115. Pujana, J., Rivero, A., Celaya, A., López de Lacalle, L.N.: Analysis of ultrasonic-assisted drilling of Ti6Al4V. Int. J. Mach. Tools Manuf **49**, 500–508 (2009). https://doi.org/10.1016/j.ijmachtools.2008.12.014
116. Young, H.-T.: Cutting temperature responses to flank wear. Wear **201**, 117–120 (1996). https://doi.org/10.1016/S0043-1648(96)07227-4
117. Kwon, P., Schiemann, T., Kountanya, R.: An inverse estimation scheme to measure steady-state tool–chip interface temperatures using an infrared camera. Int. J. Mach. Tools Manuf **41**, 1015–1030 (2001). https://doi.org/10.1016/S0890-6955(00)00113-9

118. Ekanayake, S., Isenberg, C., Schmitt, R.H.: Method for Quantitative 3D Evaluation of Defects in CFRP Using Active Lock-in Thermography. Procedia CIRP **66**, 254–258 (2017). https://doi.org/10.1016/j.procir.2017.03.368
119. Risitano, A., Risitano, G.: Cumulative damage evaluation of steel using infrared thermography. Theoret. Appl. Fract. Mech. **54**, 82–90 (2010). https://doi.org/10.1016/j.tafmec.2010.10.002
120. Usamentiaga, R., Garcia, D.F., Molleda, J., Bulnes, F.G., Orgeira, V.G.: Temperature Tracking System for Sinter Material in a Rotatory Cooler Based on Infrared Thermography. IEEE Trans. Ind. Appl. **50**, 3095–3102 (2014). https://doi.org/10.1109/TIA.2014.2306984
121. Krstulović-Opara, L., Vesenjak, M., Duarte, I., Ren, Z., Domazet, Ž: Infrared thermography as a method for energy absorption evaluation of metal foams. Mater Today Proc **3**, 1025–1030 (2016). https://doi.org/10.1016/j.matpr.2016.03.041
122. Rodríguez-Martin, M., Lagüela, S., González-Aguilera, D., Arias, P.: Cooling analysis of welded materials for crack detection using infrared thermography. Infrared Phys. Technol. **67**, 547–554 (2014). https://doi.org/10.1016/j.infrared.2014.09.025
123. Y. Gao, G.Y. Tian, P. Wang, H. Wang, Emissivity correction of eddy current pulsed thermography for rail inspection, in: 2016 IEEE Far East NDT New Technology & Application Forum (FENDT), IEEE, 2016: pp. 108–112. https://doi.org/10.1109/FENDT.2016.7992006
124. Srajbr, C., Tanasie, G., Dilger, K., Böhm, S.: Active Thermography for Quality Assurance of joints in automobile manufacturing. Weld. World **55**, 90–97 (2011). https://doi.org/10.1007/BF03321312
125. Moskovchenko, A., Švantner, M., Vavilov, V., Chulkov, A.: Analyzing probability of detection as a function of defect size and depth in pulsed IR thermography. NDT and E Int. **130**, 102673 (2022). https://doi.org/10.1016/j.ndteint.2022.102673
126. Zhang, X., Saniie, J., Heifetz, A.: Detection of defects in additively manufactured stainless steel 316L with compact infrared camera and machine learning algorithms. JOM **72**, 4244–4253 (2020). https://doi.org/10.1007/s11837-020-04428-6
127. Zhang, X., Fang, T., Saniie, J., Bakhtiari, S., Heifetz, A.: Unsupervised learning-enabled pulsed infrared thermographic microscopy of subsurface defects in stainless steel. Sci. Rep. **14**, 14865 (2024). https://doi.org/10.1038/s41598-024-64214-1
128. Accardi, E.D., Palumbo, D., Errico, V., Fusco, A., Angelastro, A., Galietti, U.: Analysing the probability of detection of shallow spherical defects by means of pulsed thermography. J Nondestr Eval **42**, 27 (2023). https://doi.org/10.1007/s10921-023-00936-y
129. E. D'Accardi, S. Altenburg, C. Maierhofer, D. Palumbo, U. Galietti, Detection of Typical Metal Additive Manufacturing Defects by the Application of Thermographic Techniques, in: The 15th International Workshop on Advanced Infrared Technology and Applications, MDPI, Basel Switzerland, 2019: p. 24. https://doi.org/10.3390/proceedings2019027024.
130. D'Accardi, E., Krankenhagen, R., Ulbricht, A., Pelkner, M., Pohl, R., Palumbo, D., Galietti, U.: Capability to detect and localize typical defects of laser powder bed fusion (L-PBF) process: an experimental investigation with different non-destructive techniques. Progress Addit. Manuf. **7**, 1239–1256 (2022). https://doi.org/10.1007/s40964-022-00297-4
131. Shi, W., Ren, Z., He, W., Hou, J., Xie, H., Liu, S.: A technique combining laser spot thermography and neural network for surface crack detection in laser engineered net shaping. Opt. Lasers Eng. **138**, 106431 (2021). https://doi.org/10.1016/j.optlaseng.2020.106431
132. Montinaro, N., Cerniglia, D., Pitarresi, G.: A numerical and experimental study through laser thermography for defect detection on metal additive manufactured parts. Frattura Ed Integrita Strutturale **12**, 231–240 (2018). https://doi.org/10.3221/IGF-ESIS.43.18
133. Chulkov, A.O., Vavilov, V.P., Kladov, DYu., Yurkina, V.A.: Thermal Nondestructive Testing of Composite and Metal Parts Manufactured by Additive Technologies. Russ. J. Nondestr. Test. **58**, 1035–1040 (2022). https://doi.org/10.1134/S1061830922700048
134. Kolb, C.G., Zier, K., Grager, J.-C., Bachmann, A., Neuwirth, T., Schmid, S., Haag, M., Axtner, M., Bayerlein, F., Grosse, C.U., Zaeh, M.F.: An investigation on the suitability of modern nondestructive testing methods for the inspection of specimens manufactured by laser powder bed fusion. SN Appl Sci **3**, 713 (2021). https://doi.org/10.1007/s42452-021-04685-3
135. Silva, H.V., Martins, A.P., Machado, M.A., Santos, T.G., Carvalho, M.S.: Double active thermographic inspection of additive manufacturing composites: numerical modelling and validation. Measurement **218**, 113212 (2023). https://doi.org/10.1016/j.measurement.2023.113212
136. J. Pierce, N.B. Crane, Impact of Pulse Length on the Accuracy of Defect Depth Measurements in Pulse Thermography, J Heat Transfer 141 (2019). https://doi.org/10.1115/1.4042785.
137. Rodríguez-Martin, M., Pisonero, J., González-Aguilera, D., Madruga, F.J.: Flash thermography to detect and evaluate impacts in polycarbonate parts produced by additive manufacturing. NDT and E Int. **146**, 103163 (2024). https://doi.org/10.1016/j.ndteint.2024.103163
138. Carvalho, M.S., Martins, A.P., Santos, T.G.: Simulation and validation of thermography inspection for components produced by additive manufacturing. Appl. Therm. Eng. **159**, 113872 (2019). https://doi.org/10.1016/j.applthermaleng.2019.113872
139. M.A. Machado, P.L. Inácio, A. Martins, M. Carvalho, R.A. Santos, A.F. Gomes, A.P. Martins, M.S. Carvalho, T.G. Santos, Inspection of composite parts produced by additive manufacturing: air-coupled ultrasound and thermography, 2019. https://www.researchgate.net/publication/335662161.
140. Notebaert, A., Quinten, J., Moonens, M., Olmez, V., Barros, C., Cunha, S.S., Demarbaix, A.: Numerical modelling of the heat source and the thermal response of an additively manufactured composite during an active thermographic inspection. Materials **17**, 13 (2023). https://doi.org/10.3390/ma17010013
141. J.R. Pierce, N.B. Crane, Preliminary Nondestructive Testing Analysis on 3D Printed Structure Using Pulsed Thermography, in: Volume 8: Heat Transfer and Thermal Engineering, American Society of Mechanical Engineers, 2017. https://doi.org/10.1115/IMECE2017-71935.
142. Shagdyrov, B.I., Chulkov, A.O., Vavilov, V.P., Kaledin, V.O., Omar, M.: Active thermal testing of impact damage in 3d-printed composite materials. Russ. J. Nondestr. Test. **56**, 1083–1090 (2020). https://doi.org/10.1134/S1061830920120098
143. de Santana, É.C., da Silva, W.F., Grosso Lima, M., Ribeiro Pereira, G., Riffel, D.B.: Three-dimensional printed subsurface defect detection by active thermography data-processing algorithm. 3D Print Addit Manuf **10**, 420–427 (2023). https://doi.org/10.1089/3dp.2021.0172
144. Saeed, N., Abdulrahman, Y., Amer, S., Omar, M.A.: Experimentally validated defect depth estimation using artificial neural network in pulsed thermography. Infrared Phys. Technol. **98**, 192–200 (2019). https://doi.org/10.1016/j.infrared.2019.03.014
145. Rodríguez-Martín, M., Fueyo, J.G., Pisonero, J., López-Rebollo, J., Gonzalez-Aguilera, D., García-Martín, R., Madruga, F.: Step heating thermography supported by machine learning and simulation for internal defect size measurement in additive

manufacturing. Measurement **205**, 112140 (2022). https://doi.org/10.1016/j.measurement.2022.112140
146. Metz, C., Franz, P., Fischer, C., Wachtendorf, V., Maierhofer, C.: Active thermography for quality assurance of 3D-printed polymer structures. Quant Infrared Thermogr J **18**, 50–71 (2021). https://doi.org/10.1080/17686733.2019.1686896
147. Moskovchenko, A., Švantner, M., Vavilov, V., Chulkov, A.: Characterizing Depth of Defects with Low Size/Depth aspect ratio and low thermal reflection by using pulsed IR thermography. Materials **14**, 1886 (2021). https://doi.org/10.3390/ma14081886
148. Montinaro, N., Cerniglia, D., Pitarresi, G.: A numerical and experimental study through laser thermography for defect detection on metal additive manufactured parts. Frattura Ed Integrità Strutturale **12**, 231–240 (2017). https://doi.org/10.3221/IGF-ESIS.43.18
149. Zhang, X., Saniie, J., Bakhtiari, S., Heifetz, A.: Compression of pulsed infrared thermography data with unsupervised learning for nondestructive evaluation of additively manufactured metals. IEEE Access **10**, 9094–9107 (2022). https://doi.org/10.1109/ACCESS.2022.3141654
150. Additive Manufacturing of Metals—Nondestructive Testing and Evaluation—Defect Detection in Parts, ASTM International, 2023. https://doi.org/10.1520/iso/astmtr52905-eb.
151. Raplee, J., Plotkowski, A., Kirka, M.M., Dinwiddie, R., Okello, A., Dehoff, R.R., Babu, S.S.: Thermographic Microstructure Monitoring in Electron Beam Additive Manufacturing. Sci. Rep. **7**, 43554 (2017). https://doi.org/10.1038/srep43554
152. H. Krauss, Qualitätssicherung beim Laserstrahlschmelzen durch schichtweise thermografische In-Process-Überwachung, 2017.
153. S. Moylan, E. Whitenton, B. Lane, J. Slotwinski, Infrared thermography for laser-based powder bed fusion additive manufacturing processes, in: AIP Conf Proc, American Institute of Physics Inc., 2014: pp. 1191–1196. https://doi.org/10.1063/1.4864956.
154. M. Reza Yavari, R.J. Williams, K.D. Cole, P.A. Hooper, P. Rao, Thermal modeling in metal additive manufacturing using graph theory: experimental validation with laser powder bed fusion using in situ infrared thermography data. J Manuf Sci Eng 142 (2020). https://doi.org/10.1115/1.4047619.
155. Lane, B., Moylan, S., Whitenton, E.P., Ma, L.: Thermographic measurements of the commercial laser powder bed fusion process at NIST. Rapid Prototyp J **22**, 778–787 (2016). https://doi.org/10.1108/RPJ-11-2015-0161
156. Mani, M., Lane, B.M., Donmez, M.A., Feng, S.C., Moylan, S.P.: A review on measurement science needs for real-time control of additive manufacturing metal powder bed fusion processes. Int. J. Prod. Res. **55**, 1400–1418 (2017). https://doi.org/10.1080/00207543.2016.1223378
157. R. Murphy, A Review of In-situ Temperature Measurements for Additive Manufacturing Technologies, in: NCSL International Workshop & Symposium Conference Proceedings 2016, NCSL International, 2016. https://doi.org/10.51843/wsproceedings.2016.11.
158. H. Krauss, T. Zeugner, M.F. Zaeh, Thermographic process monitoring in powderbed based additive manufacturing, in: AIP Conf Proc, American Institute of Physics Inc., 2015: pp. 177–183. https://doi.org/10.1063/1.4914608.
159. FLIR, The Ultimate Infrared Handbook for R&D Professionals, (2013).
160. R.B. Dinwiddie, M.M. Kirka, P.D. Lloyd, R.R. Dehoff, L.E. Lowe, G.S. Marlow, Calibrating IR cameras for in-situ temperature measurement during the electron beam melt processing of Inconel 718 and Ti-Al6-V4, in: J.N. Zalameda, P. Bison (Eds.), Thermosense: Thermal Infrared Applications XXXVIII, SPIE, 2016: p. 986107. https://doi.org/10.1117/12.2229070.
161. R.B. Dinwiddie, R.R. Dehoff, P.D. Lloyd, L.E. Lowe, J.B. Ulrich, Thermographic in-situ process monitoring of the electron-beam melting technology used in additive manufacturing, in: G.R. Stockton, F.P. Colbert (Eds.), Thermosense: Thermal Infrared Applications XXXV, SPIE, 2013: p. 87050K. https://doi.org/10.1117/12.2018412.
162. E. Rodriguez, Development Of A Thermal Imaging Feedback Control System In Electron Beam Melting, Open Access Theses & Dissertations. 1919., 2013. https://scholarworks.utep.edu/open_etd/1919.
163. Price, S., Cooper, K., Chou, K.: Evaluations of temperature measurements in powder-based electron beam additive manufacturing by near-infrared thermography. International Journal of Rapid Manufacturing **4**, 1 (2014). https://doi.org/10.1504/IJRAPIDM.2014.062010
164. T.-Y. Cheng, D. Deng, C. Herman, Curvature Effect Quantificaiton for In-Vivo IR Thermography, in: Volume 2: Biomedical and Biotechnology, American Society of Mechanical Engineers, 2012: pp. 127–133. https://doi.org/10.1115/IMECE2012-88105.
165. P. Mercelis, J.-P. Kruth, Procedure for in-situ monitoring and feedback control of selective laser powder technologies, GB 0612204.8, 2007.
166. Craeghs, T., Clijsters, S., Kruth, J.-P., Bechmann, F., Ebert, M.-C.: Detection of process failures in layerwise laser melting with optical process monitoring. Phys Procedia **39**, 753–759 (2012). https://doi.org/10.1016/j.phpro.2012.10.097
167. H. Krauss, C. Eschey, M.F. Zaeh, Thermography for Monitoring the Selective Laser Melting Process, in: University of Texas at Austin, 2012. https://doi.org/10.26153/tsw/15406.
168. Mitchell, J.A., Ivanoff, T.A., Dagel, D., Madison, J.D., Jared, B.: Linking pyrometry to porosity in additively manufactured metals. Addit. Manuf. **31**, 100946 (2020). https://doi.org/10.1016/j.addma.2019.100946
169. Oster, S., Fritsch, T., Ulbricht, A., Mohr, G., Bruno, G., Maierhofer, C., Altenburg, S.J.: On the registration of thermographic in situ monitoring data and computed tomography reference data in the scope of defect prediction in laser powder bed fusion. Metals (Basel). **12**, 947 (2022). https://doi.org/10.3390/met12060947
170. Errico, V., Palano, F., Campanelli, S.L.: Advancing powder bed fusion-laser beam technology: in-situ layerwise thermal monitoring solutions for thin-wall fabrication. Prog. Addit. Manuf (2024). https://doi.org/10.1007/s40964-024-00818-3
171. Mazzarisi, M., Angelastro, A., Latte, M., Colucci, T., Palano, F., Campanelli, S.L.: Thermal monitoring of laser metal deposition strategies using infrared thermography. J. Manuf. Process. **85**, 594–611 (2023). https://doi.org/10.1016/j.jmapro.2022.11.067
172. D'Accardi, E., Chiappini, F., Giannasi, A., Guerrini, M., Maggiani, G., Palumbo, D., Galietti, U.: Online monitoring of direct laser metal deposition process by means of infrared thermography. Prog. Addit. Manuf. **9**, 983–1001 (2024). https://doi.org/10.1007/s40964-023-00496-7
173. D'Accardi, E., Chiappini, F., Giannasi, A., Guerrini, M., Maggiani, G., Palumbo, D., Galietti, U.: On the feasibility of a predictive model of mechanical properties of AM Inconel 718 thin wallets produced by DED-LB process monitored with thermal methods, Progress in Additive Manufacturing. (2024). https://doi.org/10.1007/s40964-024-00809-4.
174. Altenburg, S.J., Scheuschner, N., Straße, A., Gumenyuk, A., Maierhofer, C.: Towards the determination of real process temperatures in the LMD process by multispectral thermography. In: Zalameda, J.N., Mendioroz, A. (eds.) Thermosense: thermal infrared applications XLIII, p. 9. SPIE (2021). https://doi.org/10.1117/12.2587881
175. Altenburg, S.J., Maierhofer, C., Straße, A., Gumenyuk, A.: Comparison of MWIR thermography and high-speed NIR thermography in a laser metal deposition (LMD) process. In: Proceedings of the 2018 international conference on quantitative infrared thermography. QIRT Council (2018). https://doi.org/10.21611/qirt.2018.p35

176. Altenburg, S.J., Straße, A., Gumenyuk, A., Maierhofer, C.: In-situ monitoring of a laser metal deposition (LMD) process: comparison of MWIR, SWIR and high-speed NIR thermography. Quant Infrared Thermogr J. **19**, 97–114 (2022). https://doi.org/10.1080/17686733.2020.1829889
177. Seppala, J.E., Migler, K.D.: Infrared thermography of welding zones produced by polymer extrusion additive manufacturing. Addit. Manuf. **12**, 71–76 (2016). https://doi.org/10.1016/j.addma.2016.06.007
178. Zhang, H., Zhao, X.: In-situ thermal monitoring informed modeling and simulation of process temperature during vat photopolymerization additive manufacturing. Mater Today Proc **70**, 237–241 (2022). https://doi.org/10.1016/j.matpr.2022.09.027
179. Renishaw, InfiniAM Spectral, (n.d.). https://www.renishaw.com/en/infiniam-spectral--42310 (accessed October 14, 2024).
180. Arcam, Arcam Brochure, (2017).
181. EOS, EOS Smart Monitoring, (n.d.). https://www.eos.info/en-us/enablement/software/eos-smart-monitoring (accessed October 14, 2024).
182. HP, HP Multi Jet Fusion Handbook, (n.d.). https://cgsplus.si/wp-content/uploads/2021/11/CGS-HP-Multi-Jet-Fusion-Handbook.pdf (accessed October 14, 2024).
183. Mabrouki, F., Genest, M., Shi, G., Fahr, A.: Numerical modeling for thermographic inspection of fiber metal laminates. NDT and E Int. **42**, 581–588 (2009). https://doi.org/10.1016/j.ndteint.2009.02.010
184. Peeters, J., Ibarra-Castanedo, C., Sfarra, S., Maldague, X., Dirckx, J.J.J., Steenackers, G.: Robust quantitative depth estimation on CFRP samples using active thermography inspection and numerical simulation updating. NDT and E Int. **87**, 119–123 (2017). https://doi.org/10.1016/j.ndteint.2017.02.003
185. Peeters, J., Ibarra-Castanedo, C., Khodayar, F., Mokhtari, Y., Sfarra, S., Zhang, H., Maldague, X., Dirckx, J.J.J., Steenackers, G.: Optimised dynamic line scan thermographic detection of CFRP inserts using FE updating and POD analysis. NDT and E Int. **93**, 141–149 (2018). https://doi.org/10.1016/j.ndteint.2017.10.006
186. Ghadermazi, K., Khozeimeh, M.A., Taheri-Behrooz, F., Safizadeh, M.S.: Delamination detection in glass–epoxy composites using step-phase thermography (SPT). Infrared Phys. Technol. **72**, 204–209 (2015). https://doi.org/10.1016/j.infrared.2015.08.006
187. Morón, C., Saiz, P., Ferrández, D., Felices, R.: Comparative analysis of infrared thermography and CFD modelling for assessing the thermal performance of buildings. Energies (Basel) **11**, 638 (2018). https://doi.org/10.3390/en11030638
188. Mukhmetov, O., Igali, D., Mashekova, A., Zhao, Y., Ng, E.Y.K., Fok, S.C., Teh, S.L.: Thermal modeling for breast tumor detection using thermography. Int. J. Therm. Sci. **161**, 106712 (2021). https://doi.org/10.1016/j.ijthermalsci.2020.106712
189. Vavilov, V.P.: Modeling thermal NDT problems. Int. J. Heat Mass Transf. **72**, 75–86 (2014). https://doi.org/10.1016/j.ijheatmasstransfer.2013.12.084
190. Hiasa, S., Birgul, R., Catbas, F.N.: Investigation of effective utilization of infrared thermography (IRT) through advanced finite element modeling. Constr. Build. Mater. **150**, 295–309 (2017). https://doi.org/10.1016/j.conbuildmat.2017.05.175
191. Rodríguez-Martín, M., Fueyo, J.G., Gonzalez-Aguilera, D., Madruga, F.J., García-Martín, R., Muñóz, Á.L., Pisonero, J.: Predictive models for the characterization of internal defects in additive materials from active thermography sequences supported by machine learning methods. Sensors **20**, 3982 (2020). https://doi.org/10.3390/s20143982
192. S. Fetni, Q.D.T. Pham, V.X. Tran, L. Duchêne, H.S. Tran, A.M. Habraken, Thermal field prediction in DED manufacturing process using Artificial Neural Network, ESAFORM 2021 (2021). https://doi.org/10.25518/esaform21.2812.
193. Krishnapillai, M., Jones, R., Marshall, I.H., Bannister, M., Rajic, N.: NDTE using pulse thermography: Numerical modeling of composite subsurface defects. Compos. Struct. **75**, 241–249 (2006). https://doi.org/10.1016/j.compstruct.2006.04.079
194. Khodayar, F., Lopez, F., Ibarra-Castanedo, C., Maldague, X.: Optimization of the inspection of large composite materials using robotized line scan thermography. J. Nondestr. Eval. **36**, 32 (2017). https://doi.org/10.1007/s10921-017-0412-x
195. Grys, S., Vokorokos, L., Borowik, L.: Size determination of subsurface defect by active thermography – Simulation research. Infrared Phys. Technol. **62**, 147–153 (2014). https://doi.org/10.1016/j.infrared.2013.11.011
196. Waugh, R.C., Dulieu-Barton, J.M., Quinn, S.: Modelling and evaluation of pulsed and pulse phase thermography through application of composite and metallic case studies. NDT and E Int. **66**, 52–66 (2014). https://doi.org/10.1016/j.ndteint.2014.04.002
197. Pastuszak, P.D.: Characterization of defects in curved composite structures using active infrared thermography. Procedia Eng **157**, 325–332 (2016). https://doi.org/10.1016/j.proeng.2016.08.373
198. Otsu, N.: A threshold selection method from gray-level histograms. IEEE Trans. Syst. Man Cybern. **9**, 62–66 (1979). https://doi.org/10.1109/TSMC.1979.4310076
199. Wallace, N.J., Crane, N.B., Jones, M.R.: Defect measurement limits using flash thermography with application to additive manufacturing. NDT and E Int. **128**, 102615 (2022). https://doi.org/10.1016/j.ndteint.2022.102615
200. Lopez, F., de Paulo Nicolau, V., Ibarra-Castanedo, C., Maldague, X.: Thermal–numerical model and computational simulation of pulsed thermography inspection of carbon fiber-reinforced composites. Int. J. Thermal Sci. **86**, 325–340 (2014). https://doi.org/10.1016/j.ijthermalsci.2014.07.015
201. Wang, Z., Pei, C., Zhang, Z., Chen, Z.: Quantitative test of delamination defects in CFRP with surface interference by laser thermography. Infrared Phys. Technol. **136**, 105046 (2024). https://doi.org/10.1016/j.infrared.2023.105046
202. Unnikrishnakurup, S., Zhang, Z., Seng, D.H.L., Zhang, Z., Pan, J., Kumar, V., Zheng, J., Manzano, C., Ngo, A.: Exploring thermal dynamics and porosity of cold-sprayed Ti-6Al-4V coatings on Al6061-T6 substrates: A pulsed thermography and numerical modeling approach. Int. J. Therm. Sci. **196**, 108732 (2024). https://doi.org/10.1016/j.ijthermalsci.2023.108732
203. Kim, C., Kang, S., Chung, Y., Kim, O., Kim, W.: Quantification of the effective detectable period for concrete voids of CLP by Lock-In thermography. Appl. Sci. **13**, 8247 (2023). https://doi.org/10.3390/app13148247
204. Chaudhuri, S., Stamm, M., Krankenhagen, R.: Weather-dependent passive thermography and thermal simulation of in-service wind turbine blades. J. Phys. Conf. Ser. **2507**, 012025 (2023). https://doi.org/10.1088/1742-6596/2507/1/012025
205. Zu, R., Yang, Y., Huang, X., Jiao, D., Zhao, J., Liu, Z.: A stress detection method for metal components based on eddy current thermography. NDT and E Int. **133**, 102762 (2023). https://doi.org/10.1016/j.ndteint.2022.102762
206. Cheng, H.-C., Chen, W.-H., Cheng, H.-F.: Theoretical and experimental characterization of heat dissipation in a board-level microelectronic component. Appl. Therm. Eng. **28**, 575–588 (2008). https://doi.org/10.1016/j.applthermaleng.2007.04.013
207. Zhang, X., Saniie, J., Cleary, W., Heifetz, A.: Quality Control of Additively Manufactured Metallic Structures with Machine Learning of Thermography Images. JOM **72**, 4682–4694 (2020). https://doi.org/10.1007/s11837-020-04408-w
208. X. Zhang, J. Saniie, A. Heifetz, Spatial Temporal Denoised Thermal Source Separation in Images of Compact Pulsed Thermography System for Qualification of Additively Manufactured Metals, in: 2021 IEEE International Conference on Electro Information

Technology (EIT), IEEE, 2021: pp. 209–214. https://doi.org/10.1109/EIT51626.2021.9491844.
209. Marani, R., Palumbo, D., Galietti, U., D'Orazio, T.: Deep learning for defect characterization in composite laminates inspected by step-heating thermography. Opt. Lasers Eng. **145**, 106679 (2021). https://doi.org/10.1016/j.optlaseng.2021.106679
210. Baumgartl, H., Tomas, J., Buettner, R., Merkel, M.: A deep learning-based model for defect detection in laser-powder bed fusion using in-situ thermographic monitoring. Prog. Addit. Manuf. **5**, 277–285 (2020). https://doi.org/10.1007/s40964-019-00108-3
211. X. Chen, H. Zhang, J. Hu, Y. Xiao, A Passive On-line Defect Detection Method for Wire and Arc Additive Manufacturing Based on Infrared Thermography, in: 2019 International Solid Freeform Fabrication Symposium, University of Texas at Austin (2019). https://doi.org/10.26153/tsw/17375.
212. Oster, S., Scheuschner, N., Chand, K., Altenburg, S.J.: Local porosity prediction in metal powder bed fusion using in-situ thermography: A comparative study of machine learning techniques. Addit. Manuf. **95**, 104502 (2024). https://doi.org/10.1016/j.addma.2024.104502
213. Oster, S., Breese, P.P., Ulbricht, A., Mohr, G., Altenburg, S.J.: A deep learning framework for defect prediction based on thermographic in-situ monitoring in laser powder bed fusion. J. Intell. Manuf. **35**, 1687–1706 (2024). https://doi.org/10.1007/s10845-023-02117-0
214. Everton, S., Dickens, P., Tuck, C., Dutton, B.: Using laser ultrasound to detect subsurface defects in metal laser powder bed fusion components. JOM **70**, 378–383 (2018). https://doi.org/10.1007/s11837-017-2661-7
215. Mandache, C.: Overview of non-destructive evaluation techniques for metal-based additive manufacturing. Mater. Sci. Technol. **35**, 1007–1015 (2019). https://doi.org/10.1080/02670836.2019.1596370
216. Forien, J.-B., Calta, N.P., DePond, P.J., Guss, G.M., Roehling, T.T., Matthews, M.J.: Detecting keyhole pore defects and monitoring process signatures during laser powder bed fusion: A correlation between in situ pyrometry and ex situ X-ray radiography. Addit. Manuf. **35**, 101336 (2020). https://doi.org/10.1016/j.addma.2020.101336
217. Segovia Ramírez, I., García Márquez, F.P., Papaelias, M.: Review on additive manufacturing and non-destructive testing. J. Manuf. Syst. **66**, 260–286 (2023). https://doi.org/10.1016/j.jmsy.2022.12.005
218. Chen, X., Kong, F., Fu, Y., Zhao, X., Li, R., Wang, G., Zhang, H.: A review on wire-arc additive manufacturing: typical defects, detection approaches, and multisensor data fusion-based model. Int. J. Adv. Manuf. Technol. **117**, 707–727 (2021). https://doi.org/10.1007/s00170-021-07807-8
219. Lu, Q.Y., Wong, C.H.: Additive manufacturing process monitoring and control by non-destructive testing techniques: challenges and in-process monitoring. Virtual Phys Prototyp **13**, 39–48 (2018). https://doi.org/10.1080/17452759.2017.1351201
220. Sreeraj, P.R., Mishra, S.K.R., Singh, P.K.: A review on non-destructive evaluation and characterization of additively manufactured components. Prog. Addit. Manuf. **7**, 225–248 (2022). https://doi.org/10.1007/s40964-021-00227-w